USGS
science for a changing world

Documentation for Assessment of Modal Pushover-Based Scaling Procedure for Nonlinear Response History Analysis of "Ordinary Standard" Bridges

By Erol Kalkan and Neal S. Kwong

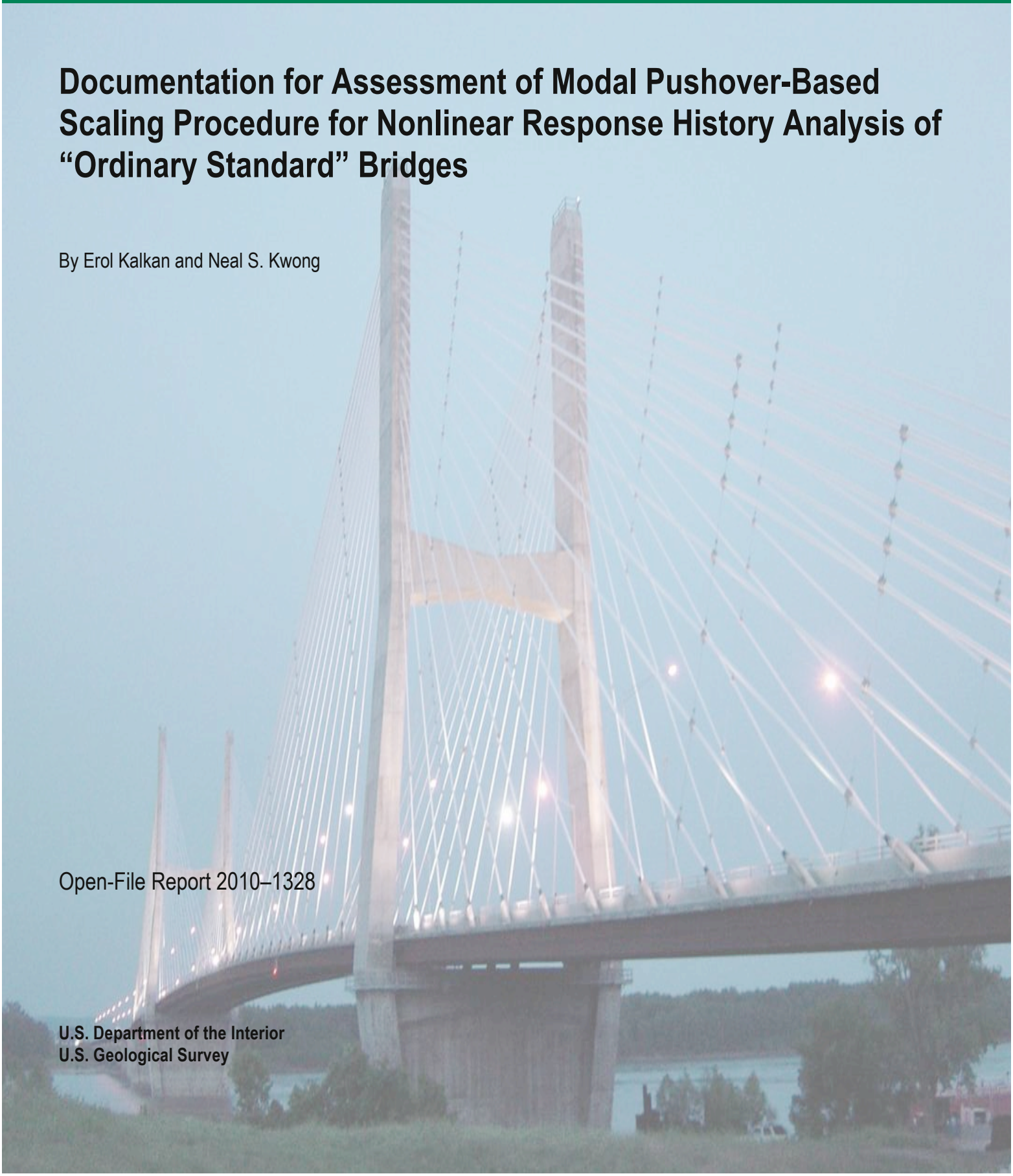

Open-File Report 2010–1328

U.S. Department of the Interior
U.S. Geological Survey

This page intentionally left blank

Documentation for Assessment of Modal Pushover-Based Scaling Procedure for Nonlinear Response History Analysis of "Ordinary Standard" Bridges

By Erol Kalkan and Neal S. Kwong

Open-File Report 2010–1328

U.S. Department of the Interior
U.S. Geological Survey

U.S. Department of the Interior
KEN SALAZAR, Secretary

U.S. Geological Survey
Marcia K. McNutt, Director
U.S. Geological Survey, Reston, Virginia 2011

For product and ordering information:
World Wide Web: *http://www.usgs.gov/pubprod/*
Telephone: 1-888-ASK-USGS

For more information on the USGS—the Federal source for science about the Earth,
its natural and living resources, natural hazards, and the environment:
World Wide Web: *http://www.usgs.gov/*
Telephone: 1-888-ASK-USGS

Suggested citation:
Kalkan, Erol, and Kwong, Neal S., 2011, Documentation for assessment of modal pushover-based scaling procedure for nonlinear response history analysis of "ordinary standard" bridges: U.S. Geological Survey Open-File Report 2010-1328, 58 p. [http://pubs.usgs.gov/of/2010/1328/].

Any use of trade, product, or firm names is for descriptive purposes only and does not imply endorsement by the U.S. Government.

Although this report is in the public domain, permission must be secured from the individual copyright owners to reproduce any copyrighted material contained within this report.

Contents

Documentation for Assessment of Modal Pushover-Based Scaling Procedure for Nonlinear Response History Analysis of "Ordinary Standard" Bridges

By Erol Kalkan[1] and Neal S. Kwong[2]

[1] U.S. Geological Survey, Menlo Park, CA 94025, *ekalkan@usgs.gov.*
[2] University of California, Berkeley, CA 94709, *nealsimonkwong@berkeley.edu*.

Abstract

The earthquake engineering profession is increasingly utilizing nonlinear response history analyses (RHA) to evaluate seismic performance of existing structures and proposed designs of new structures. One of the main ingredients of nonlinear RHA is a set of ground-motion records representing the expected hazard environment for the structure. When recorded motions do not exist (as is the case for the central United States), or when high-intensity records are needed (as is the case for San Francisco and Los Angeles), ground motions from other tectonically similar regions need to be selected and scaled. The modal-pushover-based scaling (MPS) procedure recently was developed to determine scale factors for a small number of records, such that the scaled records provide accurate and efficient estimates of "true" median structural responses. The adjective "accurate" refers to the discrepancy between the benchmark responses and those computed from the MPS procedure. The adjective "efficient" refers to the record-to-record variability of responses. Herein, the accuracy and efficiency of the MPS procedure are evaluated by applying it to four types of existing "ordinary standard" bridges typical of reinforced-concrete bridge construction in California. These bridges are the single-bent overpass, multi span bridge, curved-bridge, and skew-bridge. As compared to benchmark analyses of unscaled records using a larger catalog of ground motions, it is demonstrated that the MPS procedure provided an accurate estimate of the engineering demand parameters (EDPs) accompanied by significantly reduced record-to-record variability of the responses. Thus, the MPS procedure is a useful tool for scaling ground motions as input to nonlinear RHAs of "ordinary standard" bridges.

Introduction

Current highway bridge design practice in California is governed by the Seismic Design Criteria, SDC-2006 (Caltrans, 2006), which allows equivalent static analysis and linear elastic dynamic analysis for estimating the displacement demands, and pushover analysis for establishing the displacement capacities for "ordinary standard" bridges. For a bridge to be considered as an "ordinary standard" bridge, (1) the span length should be less than 90 m, (2) the bridge should be constructed with normal-weight concrete, (3) the foundations must be supported on spread footings, pile caps with piles, or pile shafts, and (4) the soil must not be susceptible to liquefaction or lateral spreading during strong shaking (Caltrans, 2006). More than 90 percent of bridges in California are "ordinary standard" bridges (Mark Yashinsky, personal commun.).

For "ordinary standard" bridges, analysis methods based on the linear-elastic assumption may be appropriate in regions having low-seismicity. In seismically active regions, near-fault static (surface displacement) and dynamic effects (long-period velocity pulses) may impart significant seismic demand to bridges and drive them into the inelastic range, invalidating the linear-elastic

assumption (Goel and Chopra, 2008; Kalkan and Kunnath, 2006). To portray fully the "true" nonlinear behavior of bridges to near-fault ground motions, nonlinear response history analyses (RHA) may be required. Nonlinear RHAs utilize a set of ground motions representing the hazard environment expected for the structure. When recorded motions do not exist (as is the case for the central United States), or when high-intensity records are needed (as is the case for San Francisco and Los Angeles), ground motions from other tectonically similar regions need to be selected and modified. Most of the procedures to modify ground-motion records fall into one of two categories: spectral matching (Lilhanand and Tseng, 1987, 1988) and amplitude scaling (Katsanos and others, 2010).

The objective of amplitude-scaling methods is to determine scale factors for a small number of records such that the scaled records provide an accurate estimate of "true" median structural responses and, at the same time, are efficient, that is they reduce the record-to-record variability of responses. Amplitude-scaling of records was accomplished previously by scaling them to a common intensity measure, such as peak ground acceleration (PGA), effective peak acceleration, Arias intensity, or effective peak velocity (Nau and Hall, 1984; Kurama and Farrow, 2003). These approaches generally are inaccurate and inefficient for structures responding in the inelastic range (Shome and Cornell, 1998; Kurama and Farrow, 2003). Scaling of records to a target value of the elastic spectral acceleration at a fundamental period provides improved results for structures whose response is dominated by their first-"mode" (Shome and others, 1998). However, this scaling method becomes less accurate and less efficient for structures responding significantly in their higher vibration modes or far into the inelastic range (Mehanny, 1999; Alavi and Krawinkler, 2000; Kurama and Farrow, 2003). To consider higher mode response, a vector intensity measure (IM) of first-"mode" spectral acceleration and the spectral ratio of first-"mode" and second"-mode" have been developed (Bazzurro, 1998; Shome and Cornell, 1999). Although this vector IM improves accuracy, it remains inefficient for near-fault records with a dominant velocity pulse (Baker and Cornell, 2006).

To recognize the lengthening of the apparent period of vibration due to yielding of the structure, scalar IMs have been considered (Mehanny 1999; Cordova and others, 2000). Alternatively, scaling earthquake records to minimize the difference between the elastic-response spectrum and the target spectrum has been proposed (Kennedy and others, 1984; Malhotra, 2003; Alavi and Krawinkler, 2004; Naeim and others, 2004; Youngs and others, 2007). Additional studies have suggested that selection of ground-motion records taking into account the elastic spectral shape may provide improved estimates of engineering demand parameters (EDPs) (Baker and Cornell, 2005; Mackie and Stajadinovic, 2007). The measure of spectral shape used in these studies is "epsilon", or the number of standard deviations the response spectral ordinate exceeds from a predicted median spectral value from an empirical ground-motion attenuation relation.

Because the preceding methods do not consider explicitly the inelastic behavior of the structure, they may not be appropriate for near-fault sites where the inelastic deformation can be significantly greater than the deformation of the corresponding linear system. For such sites, scaling methods that are based on the inelastic deformation spectrum or that consider the response of the first-"mode" inelastic SDF system are more appropriate (Shantz, 2006; Luco and Cornell, 2007; Tothong and Cornell, 2008; PEER, 2009).

Kalkan and Chopra (2010a, 2011) used these concepts to develop a modal pushover-based scaling (MPS) procedure for selecting and scaling earthquake ground-motion records in a form convenient for evaluating existing structures and proposed designs of new structures. This procedure explicitly considers structural strength, determined from the first-"mode" pushover curve, and determines a scaling factor for each record to match a target value of the deformation of the first-"mode" inelastic SDF system. The MPS procedure

for one-component of ground-motion has been extended for two horizontal components of ground-motion for three-dimensional analysis of structural systems (Reyes and Chopra, 2010). The MPS procedure has been proven to be accurate and efficient for low-, medium-, and high-rise symmetric-plan buildings (Kalkan and Chopra, 2010a,b, 2011; Reyes and Chopra, 2010). Here, the accuracy and efficiency of the MPS procedure are further evaluated for one- and two-components of ground-motion by applying it to four existing reinforced-concrete "ordinary standard" bridges typical of reinforced-concrete bridge construction in California. These bridges are the single-bent overpass, multi span bridge, curved-bridge, and skew-bridge responding predominantly in their first-"mode".

MPS Procedure for Bridges

The existing MPS procedure, for a single horizontal component of ground motion, scales each record by a factor such that the deformation of the first-"mode" inelastic SDF system—established from the first-"mode" pushover curve for the structure due to the scaled record—matches a target value of inelastic deformation (Kalkan and Chopra, 2010a). The target value of inelastic deformation is defined as the median deformation of the first-"mode" inelastic SDF system due to a large ensemble of unscaled ground motions compatible with the site-specific seismic hazard. The target value of inelastic deformation may be estimated by either (1) performing nonlinear RHA of the inelastic SDF system to obtain the peak deformation due to each ground motion and then computing the median of the resulting data set; or (2) multiplying the median peak deformation of the corresponding linear SDF system, known from the elastic design spectrum (or uniform hazard spectrum) by the inelastic deformation ratio, estimated from an empirical equation with known yield-strength reduction factor.

For first-"mode" dominated structures, scaling earthquake records to the same target value of the inelastic deformation is shown to be sufficient (Kalkan and Chopra, 2010a, 2011).

Summarized below is the MPS procedure as applied to bridges:

1. For the given site, define the target pseudo-acceleration response spectrum either as the probabilistic seismic hazard analysis (PSHA) based uniform hazard spectrum or code-based design spectrum, or as the median pseudo-acceleration spectrum for a large ensemble of (unscaled) earthquake records compatible with the site-specific seismic hazard conditions. For California, a Web-based tool (http://dap3.dot.ca.gov/shake_stable/index.php) is available to calculate both deterministic and probabilistic design spectrum based on the SDC-2006.

2. Compute the frequencies ω_n (periods T_n) and mode shape vectors ϕ_n of the first few modes of elastic vibration of the bridge.

3. Develop the base shear-deck displacement V_{b1}-u_{d1} relation or pushover curve by nonlinear pushover analysis of the bridge subjected gradually to increasing lateral forces with an invariant force distribution. The distribution of lateral forces is determined from the shape of the fundamental mode multiplied by tributary mass (that is, lumped mass). Gravity loads are applied before starting the pushover analysis.

4. Idealize the pushover curve and select a hysteretic model for cyclic deformations, both appropriate for the bridge's structural system and materials (Han and Chopra, 2006; Bobadilla and Chopra, 2007). Determine the yield-strength reduction factor R_y (equal to strength required for the bridge to remain elastic divided by the yield strength of the structure) from:

$R_y = M_1^* \bar{A}_1 / V_{b1y}$, where M_1^* is the effective modal mass, $\bar{A}_1$ is the target spectral acceleration (or design acceleration) at the first-"mode" and V_{b1y} is the yield point value of base shear determined from the idealized pushover curve.

5. Convert the idealized pushover curve to the force-deformation relation ($F_{s1}/L_1 - D_1$) of the first-"mode" inelastic SDF system by utilizing $F_{s1}/L_1 = V_{b1} / M_1^*$ and $D_1 = u_{d1} / \Gamma_1 \, \Phi_{d1}$ in which $L_1 = \phi_1 \mathbf{m} \iota$, Φ_{d1} is the value of $\boldsymbol{\Phi}_1$ at the deck level, u_{d1} is the deck displacement of a bridge under first-"mode" pushover, $\Gamma_1 = (\boldsymbol{\phi}_1^{\mathrm{T}} \mathbf{m} \iota) / (\boldsymbol{\phi}_1^{\mathrm{T}} \mathbf{m} \boldsymbol{\phi}_1)$ and each element of the influence vector ι is equal to unity. Note that F_{s1}/L_1 v's D_1 is simply the Acceleration Displacement Response Spectrum (ADRS) format.

6. For the first-"mode" inelastic SDF system, establish the target value of deformation $\bar{D}_1^I$ from $\bar{D}_1^I = C_R \bar{D}_1$, where $\bar{D}_1 = (T_1/2\pi)^2 \bar{A}_1 . C_R$ is determined from an empirical equation (for example, Chopra and Chintanapakdee, 2004) for the inelastic deformation ratio corresponding to the yield-strength reduction factor R_y, determined in Step 4 as:

$$C_R = 1 + \left[(L_R - 1)^{-1} + \left(\frac{a}{R_y^b} + c \right) \left(\frac{T_1}{T_c} \right)^d \right]^{-1} \quad ,(1)$$

in which, the limiting value of C_R at $T_n = 0$ is given by L_R as:

$$L_R = \frac{1}{R_y} \left(1 + \frac{R_y - 1}{\alpha} \right) \quad . \qquad (2)$$

where a is the post-yield stiffness ratio of the inelastic SDF system and T_c is the period separating the acceleration and velocity-sensitive regions of the target spectrum (for example, see right panel in figure 1); the parameters in equation (1) are: a=61, b=2.4, c=1.5, and d=2.4. Equations (1) and (2) and values of their parameters are valid for far-fault ground motions, independent of (i) earthquake magnitude and distance and (ii) National Earthquake Hazard Reduction Program (NEHRP) site class B, C, and D; and also for near-fault ground motions.

7. Compute the peak deformation $D_1^I = \max |D_1(t)|$ of the first-"mode" inelastic SDF system defined by the force deformation relation developed in Steps 4 and 5 and damping ratio ζ_1. The initial elastic vibration period of the system is $T_1 = 2\pi \, (L_1 D_{1y} / F_{s1y})^{1/2}$. For a SDF system with known T_1 and ζ_1, D_1^I can be computed by nonlinear RHA due to one of the selected ground motions $\ddot{u}_g(t)$ multiplied by a scale factor *SF*, to be determined to satisfy Step 8, by solving

$$\ddot{D}_1 + 2\zeta_1 \omega_1 \dot{D}_1 + F_{s1} D_1 / L_1 = -(SF) \ddot{u}_g(t) \quad . \qquad (3)$$

8. Compare the normalized difference between the target value of the deformation $\bar{D}_1^I$ of the first-"mode" inelastic SDF system (Step 6) and the peak deformation D_1^I, determined in Step 7 against a specified tolerance, ε

$$\Delta_1 = \left| \bar{D}_1^I - D_1^I \right| / \bar{D}_1^I < \varepsilon \quad . \qquad (4)$$

9. Determine the scale factor *SF,* such that the scaled record $(SF)\ddot{u}_g(t)$ satisfies the criterion of equation (4). Because equation (3) is nonlinear, *SF* cannot be determined

a priori, but requires an iterative procedure starting with an initial guess. Starting with *SF*=1, Steps 7 and 8 are implemented and repeated with modified values of *SF* until equation (4) is satisfied. Successive values of *SF* are chosen by trial and error or by a convergence algorithm, for example, quasi Newton iteration procedures. For a given ground motion, if equation (4) is satisfied by more than one *SF*, the *SF* closest to unity should be taken. The rationale behind this is that the applied *SF* should be limited to ensure that the scaled record does not show characteristics that would be unrealistic for the magnitude and distance pair to which it is referred.

Repeat Steps 7 and 8 for as many records as deemed necessary to obtain the scale factors *SF* for a single horizontal component of ground motion. Repeat Steps 1 through 6 to obtain a different target spectrum, pushover curve and SDF properties for the second horizontal component of ground motion. Using these items, specific to the component of ground motion, repeat Steps 7 and 8 for as many records as deemed necessary to obtain the scale factors *SF*. Note that the scale factors will be different for each record and different for each component of ground-motion for a given record (Reyes and Chopra, 2010).

If the higher modes are important for a given bridge, MPS procedure checks for second-"mode" compatibility of each record by comparing its scaled elastic spectral displacement response values at the second-"mode" vibration period of the bridge against the target spectrum. This approach ensures that each scaled earthquake record satisfies two requirements: (1) peak deformation of the first-"mode" inelastic SDF system is close enough to the target value of its inelastic deformation; and (2) that the peak deformation of the second-"mode" elastic SDF system is not far from the target spectrum. Ground-motion records satisfying these two criteria should be used in nonlinear RHA. Further details on higher mode consideration in MPS can be found in Kalkan and Chopra (2010a,b, 2011) and Reyes and Chopra (2010).

Ground Motions Selected

Twenty-one near-fault, strong earthquake ground motions were compiled from the Next Generation Attenuation project ground-motion database. These motions were recorded during seismic events with moment magnitude $6.5 \leq M \leq 7.6$ at closest fault distances $R_{cl} \leq 12$ km and belonging to NEHRP site classification C or D. The selected ground-motion records and their characteristic parameters are listed in table 1. Shown in figure 1 are the 5 percent damped response spectra of the y-component (that is, transverse direction of the bridge models) of ground motions. The median spectrum is taken as the design spectrum for purposes of evaluating the MPS procedure; also shown in this figure is the median spectrum of the ground-motion ensemble as a four-way logarithmic plot, together with its idealized version (dashed-line). Similarly, the response spectra corresponding to the x-component (that is, longitudinal direction of the bridge models) of ground motions are shown in figure 2. For a particular direction, the idealized spectrum is divided into three period ranges: the long-period region to the right of point *d*, $T_n > T_d$, is called the displacement-sensitive region; the short-period region to the left of point *c*, $T_n < T_c$, is called the acceleration-sensitive region; and the intermediate-period region between points *c* and *d*, $T_c < T_n < T_d$, is called the velocity-sensitive region (Chopra, 2007; Section 6.8). Note that the nearly constant velocity region is unusually narrow, which is typical of near-fault ground motions.

For the single-bent overpass and multi span bridge, only the y-component of ground-motion was taken into consideration for the analyses. For the curved-bridge and the skew-bridge, both horizontal components of the 21 ground-motion records were utilized. The median spectrum of records in each direction was taken as the design spectrum (that is, target spectrum).

Description of Bridges and Computer Models

In order to cover a wide variety of reinforced-concrete bridges, four types of existing "ordinary standard" bridges in California were considered: single-bent overpass, multi span bridge, curved-bridge and skew-bridge. The bird's eye views for both the single-bent overpass and multi span bridge are shown in the top row in figure 3. An isometric view of the curved-bridge and an elevation view of the skew-bridge are shown in the bottom row in figure 3.

Single-Bent Overpass

The selected bridge with a two-span continuous deck and single-bent composed of two octagonal columns is representative of an overcrossing designed according to post-Northridge Caltrans specifications. Figure 4 shows the elevation, deck and column dimensions, and column section detailing. The bridge has stub-wall abutments restrained in the longitudinal and transverse directions as a result of end-diaphragm and wing-wall interaction with the soil.

The computer model of the bridge was created in OpenSees (2009). The column bent footings were modeled as translational springs in each orthogonal direction. The abutments were modeled as restrained supports in the vertical direction and as translational springs in longitudinal and transverse directions. The stiffness of the translational springs to model the abutments was determined in accordance with the SDC-2006. The finite-element model of the bridge is represented by 3-D frame elements passing through the mid-depth of the superstructure and 3-D frame elements passing through the geometric centre and mid-depth of the columns and the cap beam. Fiber-discretized, force-based, nonlinear beam-column elements were used to model columns (fig. 5); the integration along the elements is based on Gauss-Lobatto quadrature rule. A fiber section model at each integration point, which in turn is associated with uniaxial material models and enforces the Bernoulli beam assumption for axial force and bending, represents the force-based element. Centerline dimensions were used in the element modeling for all cases. The deck elements were assumed to remain elastic based on the capacity design approach employed by the SDC-2006. The box-girder was assumed to be integral with the bent, thus full continuity was employed at the superstructure-bent connection. P-Δ effects were considered at the global level. The characteristic strength of unconfined concrete ($f_c^{'}$) was assumed to be 28 MPa with an ultimate strain of 0.005; the characteristic strength and ultimate strain of confined concrete were computed to be 41.6 MPa and 0.0169 using the model proposed by Mander and others (1988). The yield strength of both longitudinal and spiral reinforcement was specified as 413 MPa. A bilinear model with a post-yield stiffness of 1 percent of the initial stiffness was used to model the reinforcing steel. For simplicity, the columns were modeled as circular columns with a diameter of 1.65 m. The diameter of the equivalent circular column was selected such that both core and cover concrete areas of the original octagonal column are equal to those of the equivalent circular column.

Multi Span Bridge

The bridge selected is representative of typical multi span, single-frame, prestressed concrete bridges built according to post-Northridge Caltrans design specifications. Figure 6 shows the bridge elevation, deck and column dimensions, and column-section detailing. The bents of the bridge consist of single double-spiral columns.

The bridge was modeled as an elastic superstructure sitting on nonlinear columns on an elastic foundation. An overview of the computer model of the bridge is shown in figure 7. Fiber-discretized, force-based, nonlinear beam-column elements were used to model the columns while the deck elements were assumed to remain elastic. P-Δ effects were considered at the global level. The compressive strength of unconfined concrete and the yield strength of longitudinal reinforcement were taken as 28 MPa and 413 MPa, respectively.

The compressive strength and ultimate strain of confined concrete were computed as 40.2 MPa and 0.0157 using Mander's model. A bilinear model with a post-yield stiffness of 1 percent of the initial stiffness was used to model the reinforcing steel.

The columns of the bridge rest on shallow foundations. Elastic springs in three translational directions were used to model the soil effect. The approximate expressions in the ASCE 41-6 guidelines (ASCE, 2007) were used to compute properties of the corresponding spring constants. Seat-type abutments are used at both ends of the bridge. Spring systems were used to model the dynamic stiffness of the abutments. In the vertical direction, the movement of the bridge is vertically prevented at the abutments.

Curved-Bridge

The curved-bridge is representative of typical short-span, prestressed concrete bridges built in 2000 according to post-Northridge Caltrans design specifications. As illustrated in figure 3, the deck is curved, having a radius of 165 m. It has a total span length of 151.33 m, and is supported by two columns. At the abutments, sliding bearings support the bridge. The elevation view, section view, and column section detailing are shown in figure 8.

The 3-D finite-element computer model of this bridge was developed on the OpenSees platform, and a schematic representation of this model is shown in figure 9. The deck was assumed to be elastic, while the two columns were modeled as fiber-discretized, force-based, nonlinear beam-column elements. Due to the curved nature of the deck, the co-rotational geometric transformation was employed for all elements of the model. In terms of boundary conditions, the bases of the two columns were fixed. The two abutments were modeled as springs by using zero-length elements with stiffness properties in all degrees of freedom provided by the results from the neural network-based system identification technique (Lee and others, 2008). The compressive strength of unconfined concrete and the yield strength of longitudinal reinforcement were taken as 22.4 MPa and 413 MPa, respectively. The compressive strength and ultimate strain of confined concrete were computed as 25.2 MPa and 0.0238 using Mander's model. A bilinear model with a post-yield stiffness of 1 percent of the initial stiffness was used to model the reinforcing steel.

Skew-Bridge

The bridge selected is representative of typical short-span, concrete overcrossings built in 1976. An elevation view of this bridge is provided in figure 3. It has a total span length of 80.79 m and is supported by a "skewed" single bent roughly near the middle of the span. It is "skewed" in the sense that, when observed from above, the bent is not perpendicular to the deck. The bridge is supported by wing walls at the abutments. The elevation view with dimensions, section view, and column-section detailing are shown in figure 10.

The 3-D finite-element computer model of this bridge was developed on the OpenSees platform, and a schematic representation of this model is shown in figure 11. Overall, the deck was assumed to be elastic, while the bent was modeled with two fiber-discretized, nonlinear force-based beam-column elements joined by two elastic rigid beams. Each column of the bent was modeled with several nonlinear beam-column elements along the height. Additionally, the lower half of each column was modeled with a fiber section similar to section E-E, while the upper half of each column was modeled with a fiber section similar to section F-F, as shown in the lower part of figure 10. Due to the unsymmetrical plan, the co-rotational geometric transformation was employed for all elements of the model.

The bases of the two columns at the bent were fixed. The two abutments, however, were fixed in all degrees of freedom except for the translation along the longitudinal direction and the rotation about the axis parallel to the transverse direction of the bridge. Additionally, one of the abutments was free to move transversely relative to the other abutment.

The material properties were obtained from the engineering drawings; the compressive strength of unconfined concrete and the yield strength of longitudinal reinforcement were taken as 7.6 MPa and 166 MPa, respectively. The compressive strength and ultimate strain of confined concrete were computed as 9 MPa and 0.0148 by using Mander's model. We found these values are lower than typical strength values for concrete and steel used in bridge design. A bilinear model with a post-yield stiffness of 1 percent of the initial stiffness was used to model reinforcing steel.

First – "Mode" SDF-System Parameters

Figure 12 shows the first two modes of vibration and their periods for the single-bent overpass and the multi span bridge. For the single-bent overpass, the first-"mode" (0.54 s) involves a transverse translation of the deck, and the second-"mode" (0.52 s) involves a longitudinal translation of the superstructure. The multi span bridge has the first-"mode" (2.47 s) in the translational direction and second-"mode" (1.06 s) in the longitudinal direction. The transverse direction is more flexible for both bridges.

Figure 13 shows the first-"mode" (0.41 s) and the second-"mode" (0.34 s) of vibration for the curved-bridge. The first-"mode" involves translation in both the transverse and longitudinal directions of the bridge. Due to the unsymmetrical nature of the bridge, the transverse and longitudinal directions are coupled.

Figure 14 shows the first-"mode" (0.81 s) and the second-"mode" (0.51 s) of vibration for the skew-bridge. The first-"mode" involves translation primarily in the longitudinal direction of the bridge with slight movement in the transverse direction due to skewness. It is evident that the second-"mode" consists primarily of translation in the bridge's transverse direction.

Modal pushover curves for four bridges were developed in the transverse and longitudinal directions separately. Similar to the modal pushover analyses procedure for buildings (Chopra, 2007), the distribution of lateral forces was determined from the shape of the fundamental transverse mode and fundamental longitudinal mode, multiplied by tributary mass (that is, lumped mass). For the curved- and skew-bridges, the fundamental mode of the entire 3-D structure was used in determination of the distribution of lateral forces. The pushover curves were then converted to those corresponding to the equivalent SDF system by using relations described in Step 5 of the summary of the MPS procedure. For each direction, the resultant SDF pushover curves are indicated with a thick solid line in figures 15 and 16. The curves associated with the single-bent overpass and multi span bridge are illustrated in figure 15, while those associated with the curved- and skew-bridges are illustrated in figure 16. In each figure, bilinear idealization of pushover curves is shown using thick, dashed lines. For the single-bent overpass, the pushover curves are similar in the longitudinal and transverse directions. For the curved-bridge, the SDF systems in both directions have similar stiffness, but the SDF system has more strength capacity in the longitudinal direction. This will be reflected in the "exact" target value of inelastic deformation for the longitudinal direction, as will be presented later.

Evaluation of MPS Procedure

The accuracy of the MPS procedure was evaluated by comparing the median (defined as the geometric mean by assuming log-normal distribution of EDP) value of an EDP due to three sets of seven randomly selected scaled ground motions against the benchmark value, defined as the median value of the EDP due to the 21 unscaled ground motions. Although the selection process was random, no more than two records from the same event were included in a single set so that no single event is dominant within a set.

Because the 21 ground motions selected were not intense enough to drive the curved-bridge model far into the inelastic range—an obvious requirement to test any scaling procedure—both horizontal components of the 21 ground motions

were amplified by a factor of 3 and treated as "unscaled" records.

In evaluation, a scaling procedure is considered to be accurate if the median values of an EDP, due to the seven scaled ground motions are close to benchmark value; it is considered to be efficient if the dispersion of an EDP is small due to the set of seven scaled ground motions. Smaller dispersion in EDPs means a smaller number of analyses to obtain a given confidence level in the results.

The median value, $\hat{x}$ defined as the geometric mean and the dispersion measure, δ of *n* observed values of x_i are calculated from the following expressions:

$$\hat{x} = \exp\left[\frac{\sum_{i=1}^{n} \ln x_i}{n}\right] \quad ; \qquad (5)$$

$$\delta = \left[\frac{\sum_{i=1}^{n} (\ln x_i - \ln \hat{x})^2}{n-1}\right]^{1/2} . \qquad (6)$$

Benchmark Results

Figure 17 shows the benchmark EDPs for both the single-bent overpass and multi span bridge together with results from individual records to show the large record-to-record variability (that is, large dispersion). EDPs adopted here are global response parameters: peak value of deck-drift ratio (that is, deck displacement ÷ height of column) and maximum column plastic rotation over the response histories. Only the EDPs in the transverse direction were taken into consideration because it is the weakest direction for both bridges. The peak values of deck-drift ratios due to the 21 unscaled ground motions range from 1 to 5 percent, and column plastic deformations range from less than 0.01 rad to more than 0.05 rad. The deck-drift ratios are identified on the first-"mode" pushover curves in the transverse direction together with their median values in figure 18 to indicate that all of the excitations drive both bridges well into the inelastic range.

Figure 19 shows the benchmark EDPs in the transverse direction (top row) and in the longitudinal direction (bottom row) for the curved-bridge, along with results from individual records to show the large record-to-record variability. With a curved span, the terms 'longitudinal' and 'transverse' refer to the global x and y axes, respectively, that are adopted in the OpenSees model. Since the local axes for the columns in the model are set to coincide with its principal axes, and the principal axes are not in alignment with the global axes, the local axes for the columns are not in alignment with the global ones, as well. Consequently, the column plastic rotations, recorded with respect to the local axes, are not in alignment with the global axes, whereas the peak drift ratios are. Nevertheless, the column plastic rotations associated with the local axes are still referred to as transverse and longitudinal EDPs.

It can be seen in figure 19 that EDPs in the transverse direction generally are greater than those in the longitudinal direction. For peak drift ratios, the median value is 1.5 percent in the transverse direction, whereas the median value is 0.85 percent in the longitudinal direction. Similarly, for column plastic rotations, the median is 0.005 rad in the transverse direction whereas the median is 0.002 rad in the longitudinal direction. Both horizontal components of all peak drift ratios are identified on their respective first-"mode" pushover curves together with their median values in figure 20. This figure indicates that almost all excitations resulted in inelastic responses.

Figure 21 shows the benchmark EDPs in the transverse direction (top row) and in the longitudinal direction (bottom row) for the skew-bridge, along with results from individual records to highlight the large record-to-record variability. Due to the boundary conditions for this model, the EDPs in the longitudinal direction generally are much

greater than those in the transverse direction. For peak drift ratios, values in the transverse direction ranged from 0.5 percent to slightly more than 1 percent, with a median value of 0.63 percent, while those in the longitudinal direction ranged from 1 to more than 6 percent, with a median value of 2.5 percent. Similarly, for column plastic rotations, values in the transverse direction ranged from 0.002 rad to about 0.01 rad, with a median value of 0.005 rad, while those in the longitudinal direction ranged from 0.01 rad to more than 0.06 rad, with a median value of 0.023 rad. Both horizontal components of the deck-drift ratios are identified on their respective first-"mode" pushover curves together with their median values in figure 22; as shown, all excitations led to inelastic responses.

Target Value of Inelastic Deformation

In evaluation of the MPS procedure, "exact" target value of inelastic deformation $\bar{D}_1^I$ was assumed to be unknown, and it was estimated (Step 6 of the MPS procedure) by the C_R equation (Chopra and Chintanapakdee, 2004) by using the post-yield stiffness ratio (figs. 15 and 16) and yield-strength ratio. Yield-strength ratio R_y was determined (Step 4 of the MPS procedure) as 3.1 and 3.5, respectively, for the single-bent overpass and multi span bridge. Alternatively, "exact" target value of deformation $\bar{D}_1^I$ was computed by nonlinear RHAs of the first-"mode" inelastic SDF system for 21 unscaled records. Figure 23 compares the estimated target value of deformation by using the C_R equation against its "exact" value for the single-bent overpass and multi span bridge; values from individual records also are included to show record-to-record variability. In this figure, the C_R equation overestimates "exact" value of $\bar{D}_1^I$ by 12 to 14 percent.

For the curved- and skew-bridges, the use of the extended MPS procedure for two horizontal components of ground-motion (Reyes and Chopra, 2010) requires consideration of target deformation in both directions. Figure 24 compares the estimated target value by using the C_R equation against its "exact" value for both the y and x components of ground-motion for the curved-bridge. The yield-strength ratio used in the C_R equation was determined as 1.61 for the y direction. The C_R value for the x direction is set to 1 because the force required for the SDF system to remain elastic in this particular direction is less than its yield force.

Figure 25 compares the estimated target value by using the C_R equation against its "exact" value for both the y and x components of ground motions for the skew-bridge. The yield-strength ratios were determined as 6.1 and 2, respectively, for the x and y directions. It is observed that the target value of inelastic deformation $\bar{D}_1^I$ is much greater in the longitudinal direction than that in the transverse direction. For these two bridge models, the C_R equation overestimates the "exact" value of $\bar{D}_1^I$ by 9 to 18 percent in the transverse direction and by 1 to 3 percent in the longitudinal direction.

Comparisons Against Benchmark Results

Both the single-bent overpass and multi span bridge are first-"mode" dominated; the modal participation ratio for the first-"mode" is much greater than other higher modes. Thus, Steps 7 and 8 of the single-component MPS procedure are implemented to determine an appropriate scale factor for each record. The scale factors established for the single-bent overpass and multi span bridge in each of the three sets, for the y component of ground-motion only (that is, transverse direction of the bridges), are presented in table 2. The scale factors vary with the bridge model.

In the curved- and skew-bridge models, the two-component MPS procedure (Reyes and Chopra, 2010) is implemented to determine an appropriate scale factor for each horizontal component of each record. The scale factors established for the curved-bridge in each of the three sets, for both horizontal components of

ground motion, are presented in table 3. Likewise, the scale factors established for the skew-bridge in each of the three sets, for both horizontal components of ground motion, are presented in table 4. It is observed from tables 3 and 4 that all scale factors are less than 3.

The EDPs determined by nonlinear RHAs of bridges due to three sets of 7 ground motions scaled according to the MPS procedure are compared against the benchmark EDPs. Figures 26-31 exhibit these comparisons for all the bridge models. In figures 26 and 27, corresponding to the single-bent overpass and multi span bridge, respectively, only the transverse EDPs are compared. EDPs in both directions are compared for the curved-bridge in figures 28 and 29, and for the skew-bridge in figures 30 and 31.

To better examine the accuracy of the MPS procedure, ratios of median value of EDPs from the MPS procedure to the benchmark value are computed and listed in table 5 for each bridge and for each set of ground motions. For the single-bent overpass, the maximum deviation of median value of EDPs due to the MPS procedure from the benchmark value is 18 percent for the deck-drift ratio, and 21 percent for the column plastic rotation for Set 1. Sets 2 and 3 provided more accurate results with deviations ranging from 7 to 10 percent. For the multi span bridge, median deck-drift ratios due to the MPS procedure overestimate the benchmark value by a maximum of 14 percent for deck-drift ratio and 19 percent for column plastic rotation in Set 2. Using Sets 1 and 3 resulted in slightly better accuracy, with the deviations in the range of 10 to 17 percent.

Since the two-component MPS procedure is employed for the skew- and curved-bridge models, EDP ratios are computed for quantities in both the transverse and longitudinal directions. For the curved-bridge, the median values of deck-drift ratios are greater than the benchmark values by 38 percent on average in the transverse direction, and by 33 percent on average in the longitudinal direction (table 5). However, the median estimates of column plastic rotation are, on average, 105 percent greater in the transverse direction and, on average, 85 percent greater in the longitudinal direction. In this model, the median EDPs from MPS overestimate the benchmark values with the discrepancy more pronounced in the transverse direction.

In the case of the skew-bridge model, the median values of deck-drift ratios are greater than the benchmark values by 30 percent on average in the transverse direction, and by 26 percent on average in the longitudinal direction. Unlike the curved-bridge model, the discrepancies for column plastic rotations here are similar in magnitude to those for drift ratios. The column plastic rotations are, on average, 33 percent greater in the transverse direction and 24 percent greater in the longitudinal direction. In general, the deviations from benchmark values are similar in magnitude for both directions.

As evident in figures 26 through 31, the dispersion of EDPs is reduced significantly when records are scaled using the MPS procedures (compare with scatter from figs. 17, 19, and 21). To quantify this reduction, the standard deviation (δ, see equation 6) of ratio of the EDP value from each individual ground-motion to the median benchmark value is computed and listed in table 6 for each set of ground motions and for each bridge. It is apparent in table 6 that the dispersion in each set and for each bridge is much lower than that from the corresponding benchmark cases, where records are unscaled, but, are consistent with the hazard condition defined in terms of magnitude and distance.

For the single-bent overpass, the standard deviations (δ) of EDPs from the unscaled records are reduced by 39 to 77 percent using the one-component MPS procedure. For the multi span bridge, the reduction in δ is in the range of 33 to 66 percent. These results demonstrate that the one-component MPS procedure leads to scaled ground motions that yield accurate estimates of median EDPs that are accompanied with dramatically reduced dispersions, relative to the unscaled ground motions.

With regard to the curved-bridge, the reduction in δ for the EDPs is, on average, 50 percent for the transverse direction and 39 percent for the longitudinal direction. In the case of the skew-bridge, the reduction in δ for the EDPs is, on average, 60 percent for the transverse direction, and 54 percent for the longitudinal direction. These results demonstrate that scaling records with the two-component MPS procedure provides EDPs with dispersion that is significantly lower than that obtained with unscaled ground motions.

Utilizing the "exact" value of the target inelastic deformation (that is, median inelastic-deformation value as shown in fig. 23), in the one-component MPS procedure (referred to as MPS-"Exact") further improves the accuracy as shown in figures 32 and 33 for the single-bent and multi span bridges, respectively. For the single-bent overpass, the maximum deviation of median EDPs due to the MPS-"Exact" procedure from the benchmark value is 15 percent for the deck-drift ratio and 16 percent for the column plastic rotation considering Set-2 (table 5). Much better accuracy is obtained using Set 1, and excellent agreement with the benchmark values is achieved using Set 3. For the multi span bridge, median values of EDPs due to the three sets of ground motions match perfectly with the benchmark values (maximum deviation is only 6 percent).

Utilizing the "exact" value of the target inelastic deformation in both horizontal directions of ground-motion (that is, median inelastic deformation value as shown in figs. 24 and 25) in the two-component MPS procedure (referred to as MPS-"Exact") also further improves the accuracy as shown in figures 34-37 for the curved- and skew-bridges in the longitudinal and transverse directions. From the figures (plotted in the same scales), it is evident that the median value from each set is much closer to the benchmark value.

Referring to table 5 for the curved-bridge, the peak drift ratios are now only about 19 percent greater in the transverse direction and 18 percent greater in the longitudinal direction than the benchmark value. Similarly, the column plastic rotations are on average, 56 percent greater in the transverse direction and 55 percent greater in the longitudinal direction than the benchmark plastic rotations. It should be noted that, for each type of EDP, the discrepancies in both directions are similar in magnitude when MPS-"Exact" is employed.

A similar improvement in accuracy is also observed for the skew-bridge model as shown in table 5. The peak drift ratios are, on average, 19 percent greater in the transverse direction and, on average, 23 percent greater in the longitudinal direction than the benchmark drift ratio. The column plastic rotations are now roughly 21 percent greater in both directions than the benchmark plastic rotations. Similar to the curved-bridge model, the discrepancies are alike in magnitude for both directions.

As shown in table 6 for the multi span bridge, the dispersion in EDPs is further reduced (12 percent on average as compared to the MPS procedure) by utilizing the "exact" value of the target inelastic deformation for the one-component MPS procedure. A reduction in dispersion (3 percent on average) is observed in the single-bent overpass. Similarly, the dispersion in EDPs is further diminished for the skew and curved-bridges by utilizing the "exact" values of the target inelastic deformation in both directions for the two-component MPS procedure. The reduction is about 5 percent for the skew-bridge and about 4 percent for the curved-bridge.

Conclusions

Based on four "ordinary standard" bridges in California, the accuracy and efficiency of the MPS procedure (both one- and two-component versions) are assessed by comparing the median values of the engineering demand parameters (EDPs) due to three sets of seven scaled records against the benchmark values. The one-component MPS procedure was applied to the single-bent overpass and multi span bridge, while the two-component MPS procedure was applied to the curved- and skew-bridges. The efficiency of the MPS scaling

procedure was evaluated by computing the dispersion of the responses due to the seven scaled ground motions in each set and comparing it with that from the benchmark motions. This evaluation of the MPS procedures has led to the following conclusions:

1. Even for the most intense near-fault ground motions, which represent severe tests, the one-component MPS method with a small number of records estimates the median value of seismic demands to a good degree of accuracy. The maximum discrepancy is 18 percent of the benchmark value for the single-bent overpass and 14 percent of the benchmark value for the multi span bridge. The average discrepancies of 12 percent in deck-drift ratios and 14 percent in column plastic rotations for both bridges are achieved. This demonstrates the accuracy of the one-component MPS method.
2. Considering bidirectional ground excitation, the two-component MPS procedure overestimates seismic demands for bridges with irregular geometries. The level of overestimation relative to benchmark values depends more on the response quantity of interest than on the horizontal direction considered. For the curved-bridge model, the average discrepancies in column plastic rotations are greater than those for peak drift ratios. The average discrepancy for peak drift ratios is 38 percent in the transverse direction and 33 percent in the longitudinal direction. For the skew-bridge model, however, the average discrepancies for peak drift ratios are smaller: 30 percent in the transverse direction and 26 percent in the longitudinal direction.
3. The dispersion (or record-to-record variability) in the EDPs due to seven scaled records around the median is much smaller when records are scaled by both the one-component and two-component MPS procedures as compared to the unscaled records. This implies stability in the EDPs estimated from records that are scaled according to the MPS procedures relative to those obtained from unscaled records. Despite high levels of inelastic action and irregular geometries, the MPS procedures were able to reduce the scatter in estimates by about 50 percent on average. These observations indicate the efficiency of the MPS methods. It should be noted that smaller dispersion in EDPs means a smaller number of analyses to obtain a given confidence level in the results.
4. Utilizing an "exact" target value of inelastic deformation further improves the accuracy and slightly improves the efficiency. This improvement in accuracy depends, however, on the precision involved in estimating the "exact" target value of inelastic deformation. Although the additional reduction in dispersion is about 12 percent for the multi span bridge, it is less than 5 percent for all other bridge models.

As shown in this report for the "ordinary standard" bridges, the MPS procedures were accurate and efficient in reducing the number of records needed to provide stable estimates of peak displacement and plastic rotation demands from nonlinear RHA to levels practical for typical bridge-design offices. Due to complex response behavior of geometrically irregular bridges, the MPS- "Exact" procedure utilizing exact value of target inelastic deformation provides more accurate results as compared to the MPS procedure utilizing estimated value of target inelastic deformation using the C_R equation.

Readers are referred to the MPS Web site http://nsmp.wr.usgs.gov/ekalkan/MPS/index.html for further details on assessment of the one- and two component MPS methods, and for accessing MatLAB codes for scaling ground motion records using the MPS and MPS-"Exact" methods.

Acknowledgments

Erol Kalkan acknowledges the generous support of the Earthquake Engineering Research Institute for

providing him the 2008 EERI/FEMA NEHRP Professional Fellowship in Earthquake Hazard Reduction to pursue a research study on developing "Practical Guidelines to Select and Scale Earthquake Records for Nonlinear Response History Analysis of Structures"; this report is sequel to the previous study.

Special thanks are extended to Anil K. Chopra for his insightful comments. We also wish to acknowledge the generous support of Sungchil Lee, Maria Feng, Sashi K. Kunnath and Emrah Erduran with OpenSees models. Lastly, thanks to Kevin Mackie, Juan Carlos Reyes, Toorak Zokaie, and Farzin Zareian for reviewing the material presented here and providing their valuable comments and suggestions.

References Cited

Alavi, B., and Krawinkler, H., 2000, Consideration of near-fault ground motion effects in seismic design: *Proceedings of the Twelfth World Conference on Earthquake Engineering*, Paper No. 2665, Auckland, New Zealand.

Alavi, B., and Krawinkler, H., 2004, Behavior of moment-resisting frame structures subjected to near-fault ground motions: *Earthquake Engineering and Structural Dynamics,* v. 33, no. 6, p. 687-706.

American Society of Civil Engineers, 2007. ASCE 41-6 Guidelines: Seismic Rehabilitation of Existing Buildings, Reston, VA.

Baker, J.W., and Cornell, C.A., 2005, A vector-valued ground motion intensity measure consisting of spectral acceleration and epsilon: *Earthquake Engineering and Structural Dynamics*, v. 34, no. 10, p. 1193-1217.

Baker, J. W., and Cornell, A. C., 2006, Spectral shape, epsilon and record selection: *Earthquake Engineering and Structural Dynamics,* v. 35, no. 9, p. 1077-1095.

Bazzurro, P., 1998, Probabilistic Seismic Demand Analysis, Ph.D. thesis, Dept. of Civil and Env. Eng., Stanford University, CA. (Available online at http://www.rms-group.org/Thesis/PaoloBazzurro.pdf; last accessed on 06/2008).

Bobadilla, H., and Chopra, A.K., 2007, Modal Pushover Analysis for Seismic Evaluation of Reinforced Concrete Special Moment Resisting Frame Buildings: Earthquake Engineering Research Center, Report No: EERC/2007-01, 68 p.

Caltrans, 2006, Seismic Design Criteria: Version 1.4, California Department of Transportation, Sacramento, CA. (http://www.dot.ca.gov; last accessed on 06/2008).

Chopra, A.K., 2007, Dynamics of Structures: Theory and Applications to Earthquake Engineering, Prentice Hall, Englewood Cliffs, N.J.

Chopra, A. K., and Chintanapakdee, C., 2004, Inelastic Deformation Ratios for Design and Evaluation of Structures: Single-Degree-of-Freedom Bilinear Systems: *ASCE Journal of Structural Engineering*, v. 130, no. 9, p. 1304-1319.

Cordova, P.P., Deierlein, G.G., Mehanny, S.S.F. and Cornell, C.A., 2000, Development of a two-parameter seismic intensity measure and probabilistic assessment procedure: *Proceedings of the 2nd U.S.-Japan Workshop on Performance-Based Seismic Design Methodology for Reinforced Concrete Building Structures*, PEER Report 2000/10, Pacific Earthquake Engineering Research Center, University of California, Berkeley, CA.

Goel, R.K., and Chopra, A.K., 2008, Estimating Seismic Demands For "Ordinary" Bridges Crossing Fault-Rupture Zones: Earthquake Engineering Research Center, University of California at Berkeley, Report No: EERC-2008/01.

Han, S.W., and Chopra, A.K., 2006, Approximate Incremental Dynamic Analysis using the Modal Pushover Analysis Procedure: *Earthquake Engineering and Structural Dynamics*, v. 35, p. 1853-1873.

Kalkan, E., and Kunnath, S.K., 2006, Effects of Fling-Step and Forward Directivity on the Seismic Response of Buildings: *Earthquake Spectra,* v. 22, no. 2, p. 367-390.

Kalkan, E., and Chopra, A.K., 2010a, Practical Guidelines to Select and Scale Earthquake Records for Nonlinear Response History Analysis of Structures: USGS Open File Report No: 2010-1068, 126 p. (Available online at http://nsmp.wr.usgs.gov/ekalkan/MPS/index.html; last accessed on 05/2010).

Kalkan, E., and Chopra, A.K., 2010b, Evaluation of Modal Pushover-based Scaling of one Component of Ground Motion: Tall Buildings, *Earthquake Spectra* (submitted for publication; available online at http://nsmp.wr.usgs.gov/ekalkan/PDFs/Papers/J33

_Kalkan_Chopra.pdf; last accessed on 09/30/2010).

Kalkan, E., and Chopra, A. K., 2011, Modal-Pushover-based Ground Motion Scaling Procedure: *ASCE Journal of Structural Engineering*, v. 137, no. 3 (in-press; available online at http://nsmp.wr.usgs.gov/ekalkan/PDFs/Papers/J25_Kalkan_Chopra.pdf; last accessed on 05/2010).

Katsanos, E.I., Sextos, A.G., and Manolis, G.D., 2010, Selection of earthquake ground motion records: A state-of-the-art review from a structural engineering perspective: *Soil Dynamics and Earthquake Engineering*, v. 30, no. 4, p. 157-169.

Kennedy, R.P., Short, S.A., Merz, K.L., Tokarz, F.J., Idriss, I.M., Power, M.S., and Sadigh, K., 1984, Engineering characterization of ground motion-task 1: Effects of characteristics of free-field motion on structural response: NUREG/CR-3805, U.S. Regulatory Commission, Washington, D.C.

Kurama, Y., and Farrow, K., 2003, Ground motion scaling methods for different site conditions and structure characteristics: *Earthquake Engineering and Structural Dynamics*, v. 32, no. 15, p. 2425-2450.

Lee, S., Feng, M. Q., Hong, S., and Chung, Y., 2008, Long-Term Monitoring and Analysis of a Curved Concrete Box-Girder Bridge: *International Journal of Concrete Structures and Materials*, v.2, no.2, p.1-8.

Lilhanand, K., and Tseng, W.S., I987, Generation of synthetic time histories compatible with multiple-damping design response spectra: *Transactions of the 9th International Conference on Structural Mechanics in Reactor Technology*, Lausanne, K1, 105-110.

Lilhhand, K., and Tseng, W.S., 1988, Development and application of realistic earthquake time histories compatible with multiple damping design spectra: *Proceedings of the Ninth World Conference on Earthquake Engineering*, Tokyo-Kyoto, Japan, Vol. 2, pp. 819-824.

Luco, N., and Cornell, A.C., 2007, Structure-Specific Scalar Intensity Measures for Near-Source and Ordinary Earthquake Ground Motions: *Earthquake Spectra*, v. 23, no. 2, p. 357–392.

Mackie, K.R., and Stajadinovic, B., 2007, Three-Dimensional Ground Motion Scaling for Highway Bridges: *Proceedings of the 9th Canadian Conference on Earthquake Engineering*, Ottawa, Canada, 26-29 June.

Malhotra, P.K., 2003, Strong-Motion Records for Site-Specific Analysis: *Earthquake Spectra*, v. 19, no. 3, p. 557-578.

Mander, J.B., Priestley M.J.N., and Park, R., 1988, Theoretical stress–strain model for confined concrete: *ASCE Journal of Structural Engineering*, v. 114, no. 8, p.1804–26.

Mehanny, S.S.F., 1999, Modeling and Assessment of Seismic Performance of Composite Frames with Reinforced Concrete Columns and Steel Beams, Ph.D. thesis, Department of Civil and Environmental Engineering, Stanford University, California.

Naeim, F., Alimoradi, A., and Pezeshk, S., 2004, Selection and scaling of ground motion time histories for structural design using genetic algorithms: *Earthquake Spectra*, v. 20, no. 2, p. 413-426.

Nau, J., and Hall, W., 1984, Scaling methods for earthquake response spectra: *ASCE Journal of Structural Engineering*, v. 110, no. 91-109.

OpenSees. Open Source finite element platform for earthquake engineering simulations, 2009, University of California Berkeley, Pacific Earthquake Engineering Center. (Available online at http://OpenSees.berkeley.edu/; last accessed on 06/2009).

PEER Ground Motion Selection and Modification Working Group, 2009, Evaluation of Ground Motion Selection and Modification Methods: Predicting Median Interstory Drift Response of Buildings, Haselton, C.B. (editor): PEER Report No. 2009/01, University of California, Berkeley, CA.

Reyes, J.C., and Chopra, A.K., 2010, Modal Pushover-Based Scaling of Two Components of Ground Motion Records for Nonlinear RHA of Buildings, (submitted for publication).

Shantz, T.J., 2006, Selection and scaling of earthquake records for nonlinear dynamic analysis of first-"mode" dominant bridge structures: *Proceedings of the Eighth U.S. National Conference on Earthquake Engineering,* San Francisco, CA.

Shome, N., and Cornell, A.C., 1998, Normalization and scaling accelerograms for nonlinear structural analysis: *Proceedings of the Sixth U.S. National Conference on Earthquake Engineering*, Seattle, WA.

Shome, N., Cornell, C.A., Bazzurro, P., and Carballo, J. E., 1998, Earthquakes, records and nonlinear responses, *Earthquake Spectra*, v. 14, no.3, p. 469–500.

Shome, N., and Cornell, C.A., 1999, Probabilistic Seismic Demand Analysis of Nonlinear Structures: Reliability of Marine Structures Program Report No. RMS-35, Deptartment of Civil and Env. Eng., Stanford University, CA. (Available online at http://www.rms-group.org/Thesis/NileshShome.pdf; last accessed on 01/2011).

Tothong, P., and Cornell, A.C., 2008, Structural performance assessment under near-source pulse-like ground motions using advanced ground motion intensity measures: *Earthquake Engineering and Structural Dynamics*, v. 37, no. 7, p. 1013-1037.

Youngs, R. Power, M., Wang, G., Makdisi, F. and Chin, C.C., 2007, Design Ground Motion Library (DGML) – Tool for Selecting Time History Records for Specific Engineering Applications (Abstract)," SMIP07 Seminar on Utilization of Strong-Motion Data, p. 109 – 110. (Available online at http://www.conservation.ca.gov/cgs/smip/docs/seminar/SMIP07/Pages/Paper8_Youngs.aspx; last accessed on 01/2010).

Notation

The following symbols are used in this report:

$\overline{\mathrm{A}}_{\mathrm{n}}$	Target pseudo-spectral acceleration
C_R	Ratio of peak deformations of inelastic and corresponding elastic SDF systems for systems with known yield-strength reduction factor
$\overline{D}_n$	Target value of nth mode elastic deformation
$\overline{D}_1^I$	First-"mode" target value of inelastic spectral displacement
$D_n(\mathrm{t})$	Deformation of a SDF system
D_1^I	Peak deformation of inelastic SDF system
D_n	Peak deformation of elastic SDF system
$D_{1,y}$	Yield deformation of inelastic SDF system
F_{s1}	System resisting force under first-"mode" pushover
$\mathbf{m}$	Mass matrix of a MDF system
M	Moment magnitude of earthquake
M^*	Effective modal mass
n	Mode sequence number
R_y	Yield-strength reduction factor
$\mathrm{R}_{\mathrm{rup}}$	Closest distance to co-seismic rupture plane
$\boldsymbol{s}_{\boldsymbol{n}}^*$	Load vector of modal pushover analysis
SF	Ground-motion scaling factor
T_n	Elastic natural vibration period
T_c	Period separating acceleration and velocity-sensitive regions of the spectrum
u_{d1}	Deck displacement of a bridge under first-"mode" pushover
$\ddot{u}_g$	Earthquake ground acceleration
V_{b1}	Base shear under first-"mode" pushover
V_{b1y}	Global yield strength under first-"mode" pushover
$\mathrm{V}_{\mathrm{S30}}$	Average shear-wave velocity within 30m depth from surface
α	Ratio of post-yield and initial stiffness
ζ	Damping ratio
Γ	Modal participation factor
$\boldsymbol{\phi}$	Mode shape
$\boldsymbol{\iota}$	Influence vector

Table 1. Selected near-fault intense ground-motion records [M, magnitude; R_{rup}, closest distance to coseismic rupture plane; V_{S30}, average shear-wave velocity within upper 30 m of surface].

Record No.	Earthquake Name	Year	Recording Station	M	R_{rup} (km)	V_{S30} (m/s)
1	Tabas, Iran	1978	Tabas	7.4	2.1	767
2	Imperial Valley, Calif.	1979	El Centro Meloland Overpass Free Field	6.5	0.1	186
3	Imperial Valley, Calif.	1979	El Centro Array No. 7	6.5	0.6	211
4	Superstition Hills, Calif.	1987	Parachute Test Site	6.5	1.0	349
5	Loma Prieta, Calif.	1989	LGPC	6.9	3.9	478
6	Erzincan, Turkey	1992	Erzincan	6.7	4.4	275
7	Northridge, Calif.	1994	Jensen Filter Plant	6.7	5.4	373
8	Northridge, Calif.	1994	Newhall - W. Pico Canyon Road	6.7	5.5	286
9	Northridge, Calif.	1994	Rinaldi Receiving Station	6.7	6.5	282
10	Northridge, Calif.	1994	Sylmar - Converter Station	6.7	5.4	251
11	Northridge, Calif.	1994	Sylmar - Converter Station East	6.7	5.2	371
12	Northridge, Calif.	1994	Sylmar - Olive View Medical Center Free Field	6.7	5.3	441
13	Kobe, Japan	1995	Port Island	6.9	3.3	198
14	Kobe, Japan	1995	Takatori	6.9	1.5	256
15	Kocaeli, Turkey	1999	Yarimca	7.4	4.8	297
16	Chi-Chi, Taiwan	1999	TCU052	7.6	0.7	579
17	Chi-Chi, Taiwan	1999	TCU065	7.6	0.6	306
18	Chi-Chi, Taiwan	1999	TCU068	7.6	0.3	487
19	Chi-Chi, Taiwan	1999	TCU084	7.6	11.2	553
20	Chi-Chi, Taiwan	1999	TCU102	7.6	1.5	714
21	Duzce, Turkey	1999	Duzce	7.2	6.6	276

Table 2. Scale factors computed for ground-motion records considering modal pushover-based scaling (MPS) procedure and MPS-"Exact" procedure for single-bent overpass and multi span bridge.

				MPS *		MPS-"Exact" **	
Set No.	Record No.	Earthquake Name	Recording Station	Single-Bent Overpass	Multi Span Bridge	Single-Bent Overpass	Multi Span Bridge
1	1	Superstition Hills, Calif.	Parachute Test Site	1.10	1.07	1.05	0.96
1	2	Northridge, Calif.	Jensen Filter Plant	0.87	1.06	0.80	0.96
1	3	Northridge, Calif.	Sylmar - Converter Station East	1.44	1.54	1.37	1.39
1	4	Kobe, Japan	Takatori	0.92	1.04	0.89	0.94
1	5	Chi-Chi, Taiwan	TCU065	1.28	0.96	1.17	0.90
1	6	Chi-Chi, Taiwan	TCU102	1.58	1.38	1.47	1.24
1	7	Kocaeli, Turkey	Yarimca	2.56	2.04	2.52	1.90
2	1	Erzincan, Turkey	Erzincan	1.14	1.26	1.11	1.16
2	2	Imperial Valley, Calif.	El Centro Meloland Overpass Free Field	2.05	1.30	1.94	1.18
2	3	Kobe, Japan	Port Island	1.42	1.20	1.35	1.09
2	4	Northridge, Calif.	Sylmar - Converter Station	0.80	1.14	0.73	1.01
2	5	Tabas, Iran	Tabas	1.17	1.14	1.11	1.05
2	6	Chi-Chi, Taiwan	TCU052	1.33	0.98	1.29	0.87
2	7	Chi-Chi, Taiwan	TCU084	0.38	1.00	0.35	0.89
3	1	Duzce, Turkey	Duzce	1.96	1.45	1.86	1.34
3	2	Imperial Valley, Calif.	El Centro Array No. 7	1.27	1.21	1.19	1.17
3	3	Loma Prieta, Calif.	LGPC	1.57	0.87	1.52	0.81
3	4	Northridge, Calif.	Rinaldi Receiving Station	0.63	1.14	0.57	1.03
3	5	Northridge, Calif.	Sylmar - Olive View Medical Center Free Field	1.23	1.60	1.20	1.46
3	6	Chi-Chi, Taiwan	TCU068	1.33	0.67	1.24	0.62
3	7	Northridge, Calif.	Newhall - W. Pico Canyon Road	0.94	0.79	0.91	0.72

*Target inelastic deformation is computed by using the C_R equation.

**"Exact" value of target inelastic deformation is used.

Table 3. Scale factors computed for ground-motion records considering modal pushover-based scaling (MPS) procedure and MPS-"Exact" procedure for curved-bridge for both horizontal components of ground motion.

				MPS *		MPS-"Exact" **	
Set No.	Record No.	Earthquake Name	Recording Station	Transverse Direction	Longitudinal Direction	Transverse Direction	Longitudinal Direction
1	1	Superstition Hills, Calif.	Parachute Test Site	1.60	1.24	1.40	1.24
1	2	Northridge, Calif.	Jensen Filter Plant	1.10	1.33	0.93	1.33
1	3	Northridge, Calif.	Sylmar - Converter Station East	1.04	1.46	0.87	1.46
1	4	Kobe, Japan	Takatori	1.12	0.82	0.94	0.82
1	5	Chi-Chi, Taiwan	TCU065	1.71	1.20	1.50	1.20
1	6	Chi-Chi, Taiwan	TCU102	2.31	2.71	2.11	2.71
1	7	Kocaeli, Turkey	Yarimca	2.64	1.70	2.25	1.70
2	1	Erzincan, Turkey	Erzincan	1.64	1.21	1.40	1.21
2	2	Imperial Valley, Calif.	El Centro Meloland Overpass Free Field	2.00	1.65	1.73	1.65
2	3	Kobe, Japan	Port Island	2.24	1.85	2.00	1.85
2	4	Northridge, Calif.	Sylmar - Converter Station	1.43	0.71	1.24	0.71
2	5	Tabas, Iran	Tabas	0.95	0.64	0.80	0.64
2	6	Chi-Chi, Taiwan	TCU052	1.99	1.38	1.79	1.38
2	7	Chi-Chi, Taiwan	TCU084	0.73	1.13	0.61	1.13
3	1	Duzce, Turkey	Duzce	1.68	0.75	1.46	0.75
3	2	Imperial Valley, Calif.	El Centro Array No. 7	1.43	2.11	1.22	2.11
3	3	Loma Prieta, Calif.	LGPC	0.99	0.93	0.83	0.93
3	4	Northridge, Calif.	Rinaldi Receiving Station	0.66	0.98	0.56	0.98
3	5	Northridge, Calif.	Sylmar - Olive View Medical Center Free Field	0.70	0.89	0.52	0.89
3	6	Chi-Chi, Taiwan	TCU068	1.01	1.47	0.85	1.47
3	7	Northridge, Calif.	Newhall - W. Pico Canyon Road	1.61	1.45	1.45	1.45

*Target inelastic deformation is computed by using the C_R equation.

**"Exact" value of target inelastic deformation is used.

Table 4. Scale factors computed for ground-motion records considering modal pushover-based scaling (MPS) procedure and MPS-"Exact" procedure for skew-bridge for both horizontal components of ground motion.

				MPS *		MPS-"Exact" **	
Set No.	Record No.	Earthquake Name	Recording Station	Transverse Direction	Longitudinal Direction	Transverse Direction	Longitudinal Direction
1	1	Superstition Hills, Calif.	Parachute Test Site	1.61	1.44	1.47	1.40
1	2	Northridge, Calif.	Jensen Filter Plant	1.04	1.16	0.96	1.13
1	3	Northridge, Calif.	Sylmar - Converter Station East	1.05	0.99	0.96	0.96
1	4	Kobe, Japan	Takatori	1.29	0.45	1.21	0.44
1	5	Chi-Chi, Taiwan	TCU065	1.53	0.68	1.40	0.67
1	6	Chi-Chi, Taiwan	TCU102	1.95	1.24	1.79	1.23
1	7	Kocaeli, Turkey	Yarimca	2.61	1.31	2.39	1.27
2	1	Erzincan, Turkey	Erzincan	1.57	1.61	1.46	1.57
2	2	Imperial Valley, Calif.	El Centro Meloland Overpass Free Field	1.92	1.55	1.78	1.51
2	3	Kobe, Japan	Port Island	1.92	1.10	1.79	1.09
2	4	Northridge, Calif.	Sylmar - Converter Station	1.12	1.13	1.02	1.11
2	5	Tabas, Iran	Tabas	0.82	0.71	0.75	0.70
2	6	Chi-Chi, Taiwan	TCU052	1.81	0.79	1.67	0.77
2	7	Chi-Chi, Taiwan	TCU084	0.70	1.36	0.65	1.34
3	1	Duzce, Turkey	Duzce	1.48	2.01	1.38	1.98
3	2	Imperial Valley, Calif.	El Centro Array No. 7	1.31	1.47	1.20	1.46
3	3	Loma Prieta, Calif.	LGPC	0.87	2.17	0.80	2.14
3	4	Northridge, Calif.	Rinaldi Receiving Station	0.60	1.27	0.55	1.25
3	5	Northridge, Calif.	Sylmar - Olive View Medical Center Free Field	0.82	1.09	0.75	1.06
3	6	Chi-Chi, Taiwan	TCU068	0.96	0.73	0.88	0.73
3	7	Northridge, Calif.	Newhall - W. Pico Canyon Road	1.39	1.69	1.29	1.68

*Target inelastic deformation is computed by using the C_R equation.

**"Exact" value of target inelastic deformation is used.

Table 5. Comparison of engineering demand parameter (EDP) ratios considering modal pushover-based scaling (MPS) procedure and MPS-"Exact" procedure for four bridges and for three sets of seven ground-motion records.

	Single-Bent Overpass					
	MPS			MPS-"Exact"		
EDP Ratio (MPS Median ÷ Benchmark)	**Set-1**	**Set-2**	**Set-3**	**Set-1**	**Set-2**	**Set-3**
Deck-Drift	1.18	0.93	1.08	1.08	0.85	1.00
Column Plastic Rotation	1.21	0.93	1.10	1.10	0.84	1.01

	Multi Span Bridge					
	MPS			MPS-"Exact"		
EDP Ratio (MPS Median ÷ Benchmark)	**Set-1**	**Set-2**	**Set-3**	**Set-1**	**Set-2**	**Set-3**
Deck-Drift	1.12	1.14	1.10	1.04	1.00	1.02
Column Plastic Rotation	1.17	1.19	1.13	1.06	1.00	1.04

	Curved-Bridge					
	MPS			MPS-"Exact"		
EDP Ratio (MPS Median ÷ Benchmark)	**Set-1**	**Set-2**	**Set-3**	**Set-1**	**Set-2**	**Set-3**
Deck-Drift (Transverse)	1.32	1.48	1.35	1.16	1.26	1.14
Column Plastic Rotation (Transverse)	1.99	2.25	1.91	1.57	1.74	1.38
Deck-Drift (Longitudinal)	1.29	1.42	1.29	1.15	1.27	1.12
Column Plastic Rotation (Longitudinal)	1.79	2.09	1.67	1.53	1.80	1.32

	Skew-Bridge					
	MPS			MPS-"Exact"		
EDP Ratio (MPS Median ÷ Benchmark)	**Set-1**	**Set-2**	**Set-3**	**Set-1**	**Set-2**	**Set-3**
Deck-Drift (Transverse)	1.34	1.30	1.25	1.22	1.20	1.14
Column Plastic Rotation (Transverse)	1.37	1.35	1.28	1.22	1.25	1.15
Deck-Drift (Longitudinal)	1.20	1.30	1.29	1.14	1.27	1.27
Column Plastic Rotation (Longitudinal)	1.24	1.25	1.24	1.17	1.24	1.22

Table 6. Comparison of dispersion measures considering modal pushover-based scaling (MPS) procedure and MPS-"Exact" procedure for four bridges and for three sets of seven ground-motion records.

	Single-Bent Overpass						
		MPS			MPS-"Exact"		
Dispersion Measure (δ)	**Benchmark**	**Set-1**	**Set-2**	**Set-3**	**Set-1**	**Set-2**	**Set-3**
Deck-Drift	0.52	0.12	0.31	0.22	0.13	0.29	0.21
Column Plastic Rotation	0.56	0.13	0.34	0.24	0.14	0.32	0.23

	Multi Span Bridge						
		MPS			MPS-"Exact"		
Dispersion Measure (δ)	**Benchmark**	**Set-1**	**Set-2**	**Set-3**	**Set-1**	**Set-2**	**Set-3**
Deck-Drift	0.40	0.26	0.21	0.14	0.21	0.17	0.14
Column Plastic Rotation	0.45	0.30	0.27	0.16	0.28	0.22	0.15

	Curved-Bridge						
		MPS			MPS-"Exact"		
Dispersion Measure (δ)	**Benchmark**	**Set-1**	**Set-2**	**Set-3**	**Set-1**	**Set-2**	**Set-3**
Deck-Drift (Transverse)	0.51	0.29	0.29	0.28	0.29	0.31	0.24
Column Plastic Rotation (Transverse)	1.15	0.46	0.46	0.56	0.49	0.47	0.55
Deck-Drift (Longitudinal)	0.47	0.31	0.31	0.27	0.31	0.29	0.24
Column Plastic Rotation (Longitudinal)	1.08	0.60	0.70	0.57	0.54	0.67	0.52

	Skew-Bridge						
		MPS			MPS-"Exact"		
Dispersion Measure (δ)	**Benchmark**	**Set-1**	**Set-2**	**Set-3**	**Set-1**	**Set-2**	**Set-3**
Deck-Drift (Transverse)	0.47	0.16	0.20	0.19	0.15	0.17	0.17
Column Plastic Rotation (Transverse)	0.57	0.30	0.19	0.23	0.27	0.12	0.20
Deck-Drift (Longitudinal)	0.95	0.47	0.39	0.39	0.47	0.38	0.38
Column Plastic Rotation (Longitudinal)	0.71	0.40	0.27	0.33	0.40	0.29	0.32

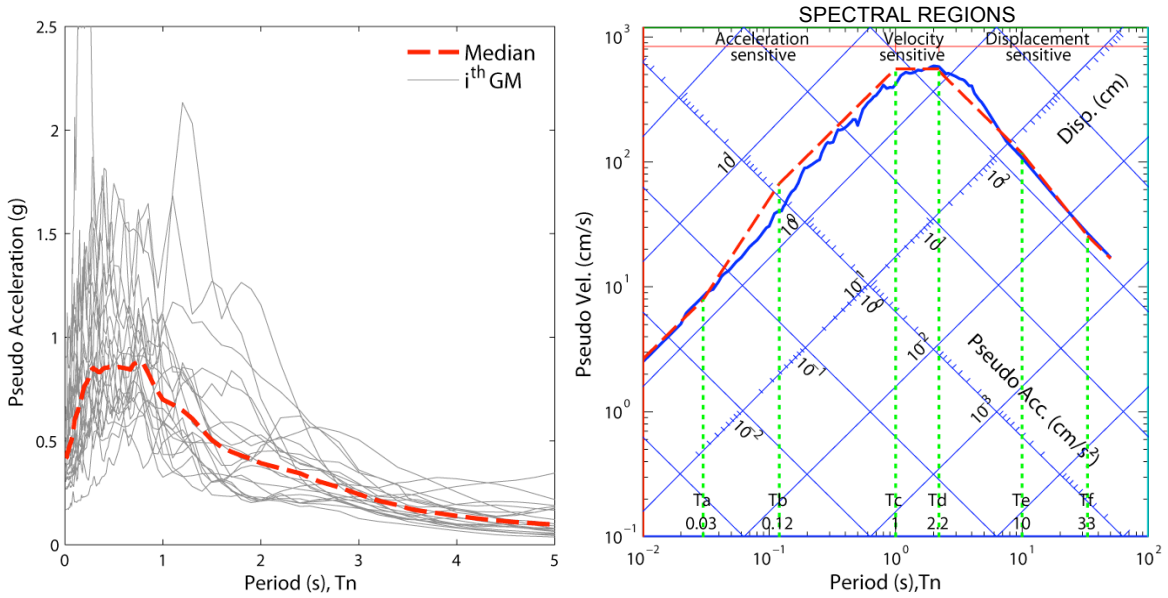

Figure 1. [Left] Individual response spectra for 21 unscaled ground-motion records and their median response spectrum taken as the design spectrum. [Right] Median elastic-response spectrum (that is, design spectrum) for the selected ensemble of ground motions shown by a solid line, together with its idealized version in dashed line; spectral regions also are identified. Damping ratio, ζ = 5 percent. Plots are for the "y-component" of the ground-motion records (that is, transverse direction of bridge models).

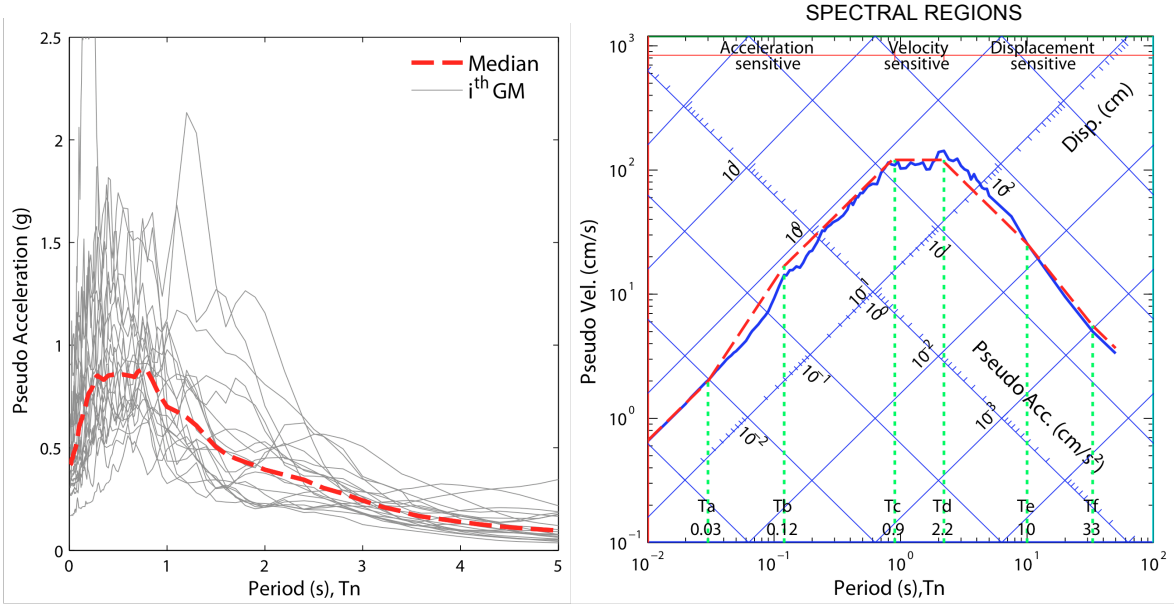

Figure 2. [Left] Individual response spectra for 21 unscaled ground-motion records and their median response spectrum taken as the design spectrum. [Right] Median elastic-response spectrum for the selected ensemble of ground-motion records shown by a solid line, together with its idealized version in dashed line; spectral regions also are identified. Damping ratio, ζ = 5 percent. Plots are for the "x-component" of the ground-motion records (that is, longitudinal direction of bridge models).

Figure 3. Bird's eye views for single-bent overpass [top-left] and multi span bridge [top-right]; isometric view for curved-bridge [bottom-left] and elevation view for skew-bridge [bottom-right]; all four "ordinary standard" reinforced-concrete bridges are located in California.

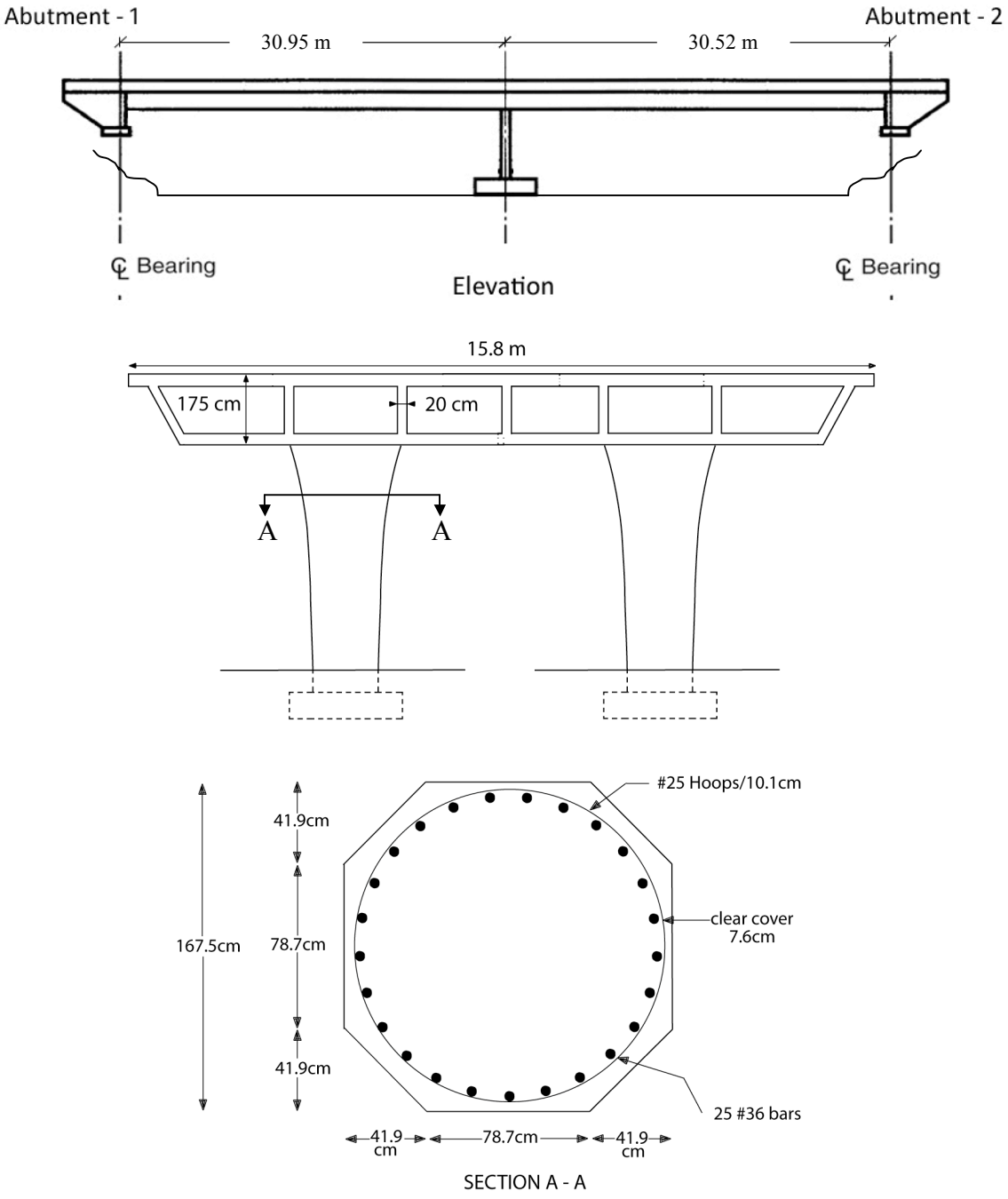

Figure 4. Elevation, deck and column dimensions, and column-section details of the single-bent overpass.

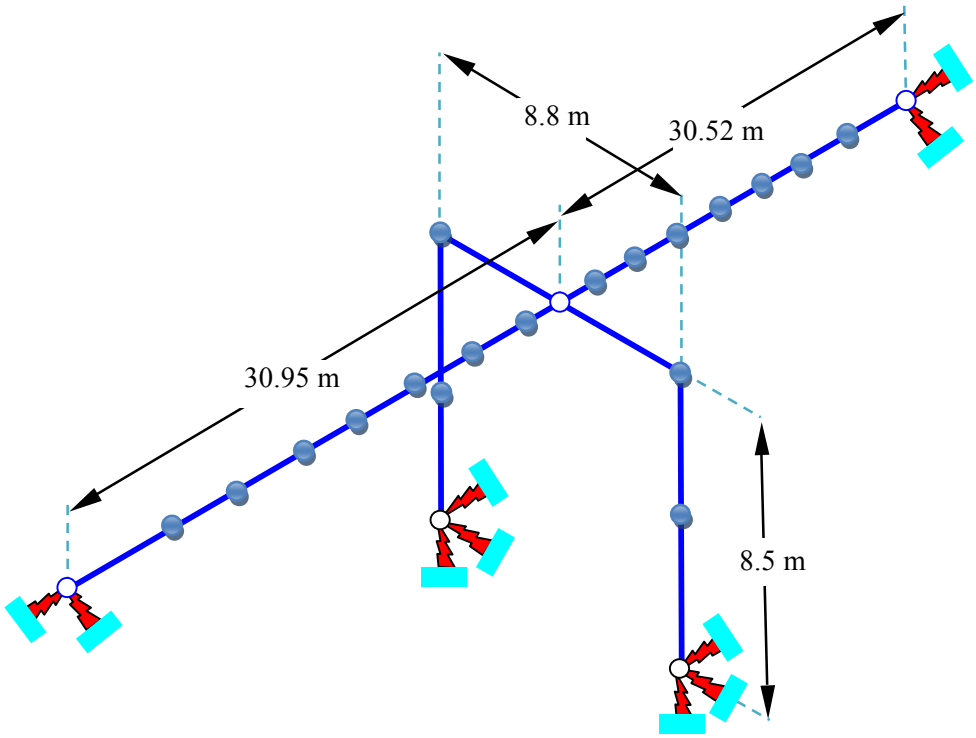

Figure 5. Idealized computer model of the single-bent overpass.

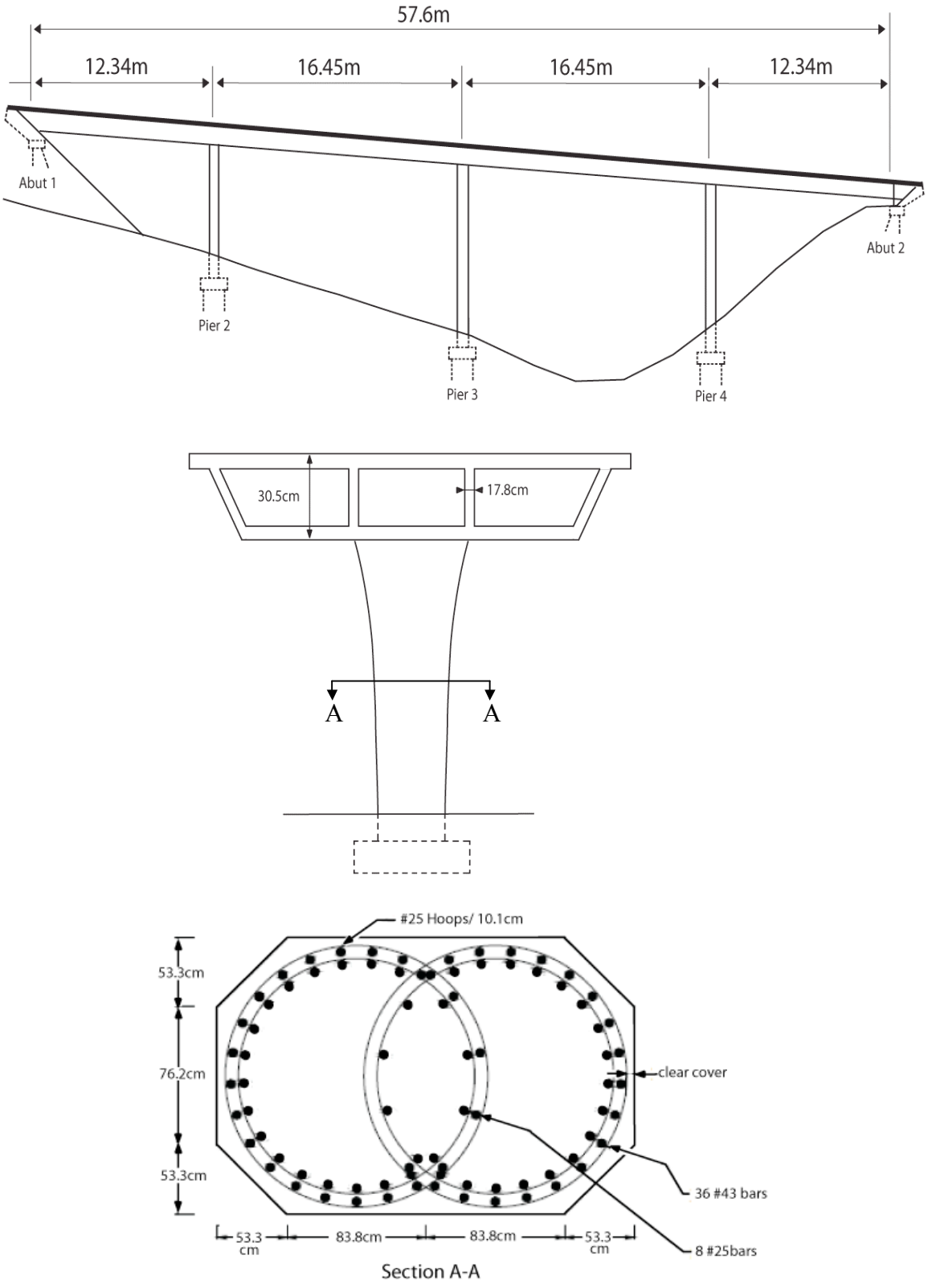

Figure 6. Elevation, deck and column dimensions, and column-section details of the multi span bridge.

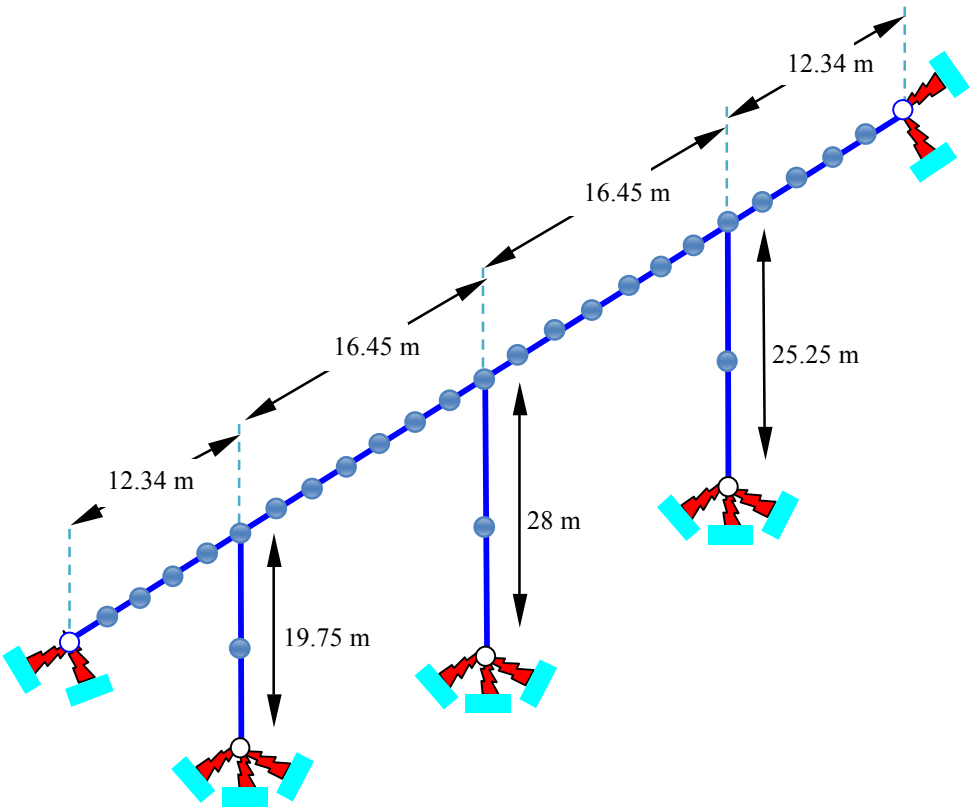

Figure 7. Idealized computer model of the multi span bridge.

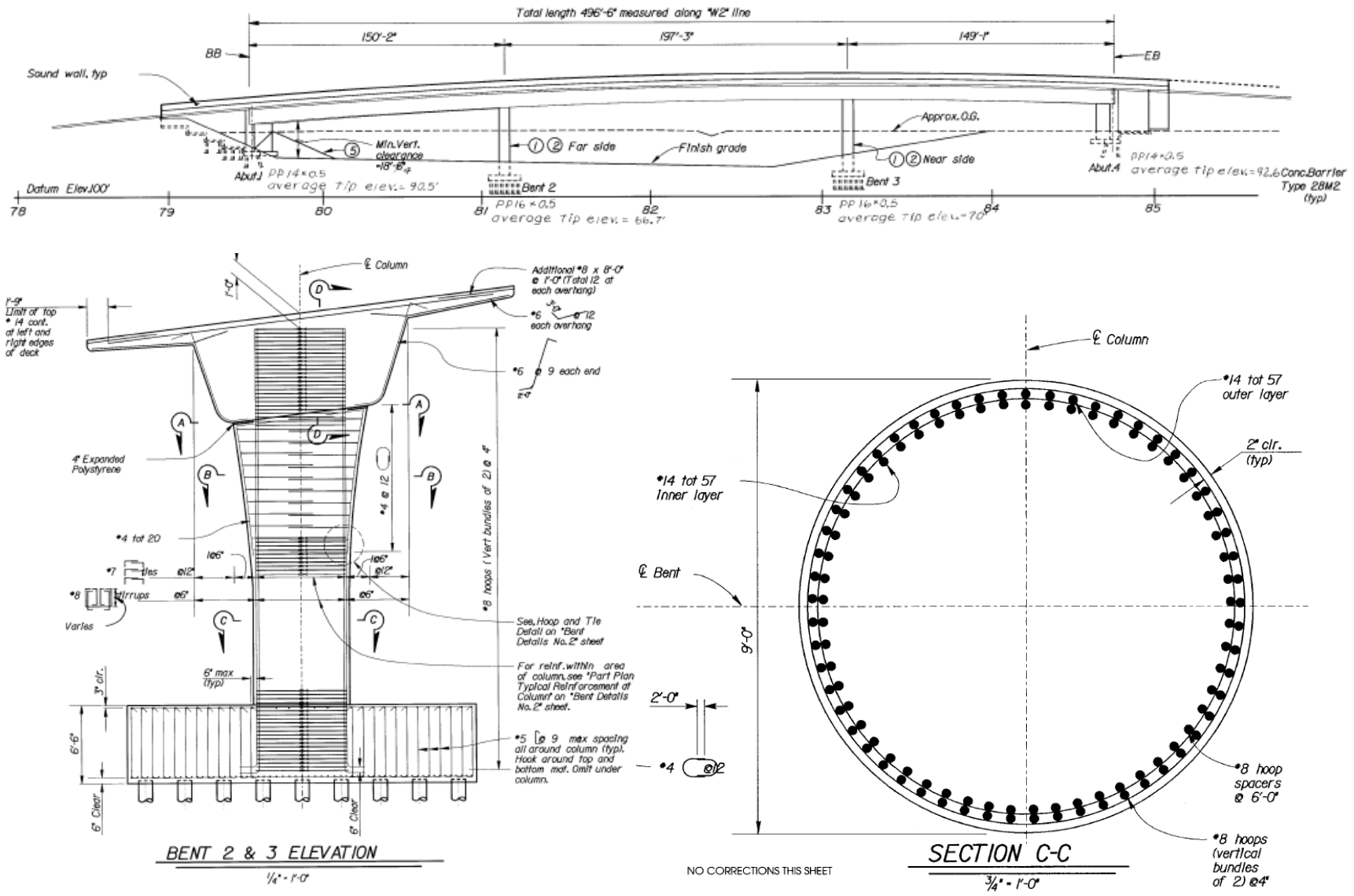

Figure 8. Elevation, deck and column dimensions, and column-section details of the curved-bridge.

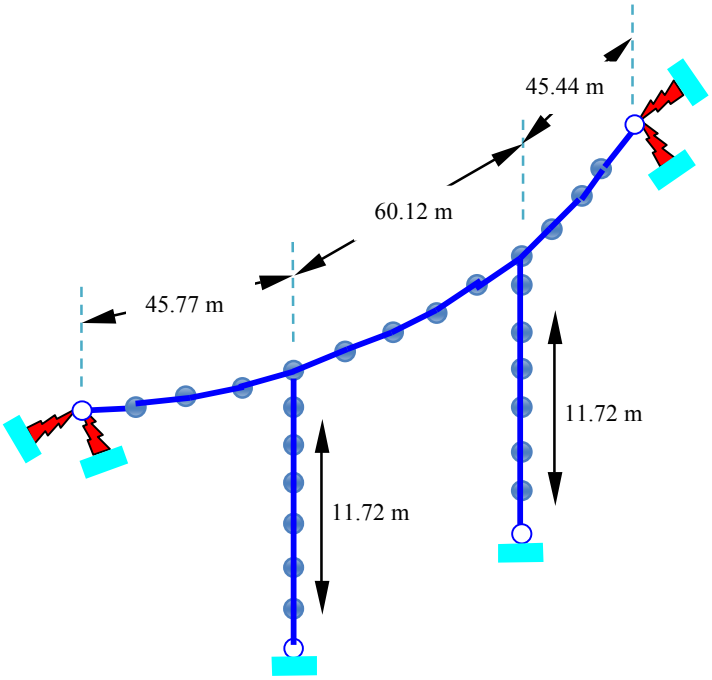

Figure 9. Idealized computer model of the curved-bridge.

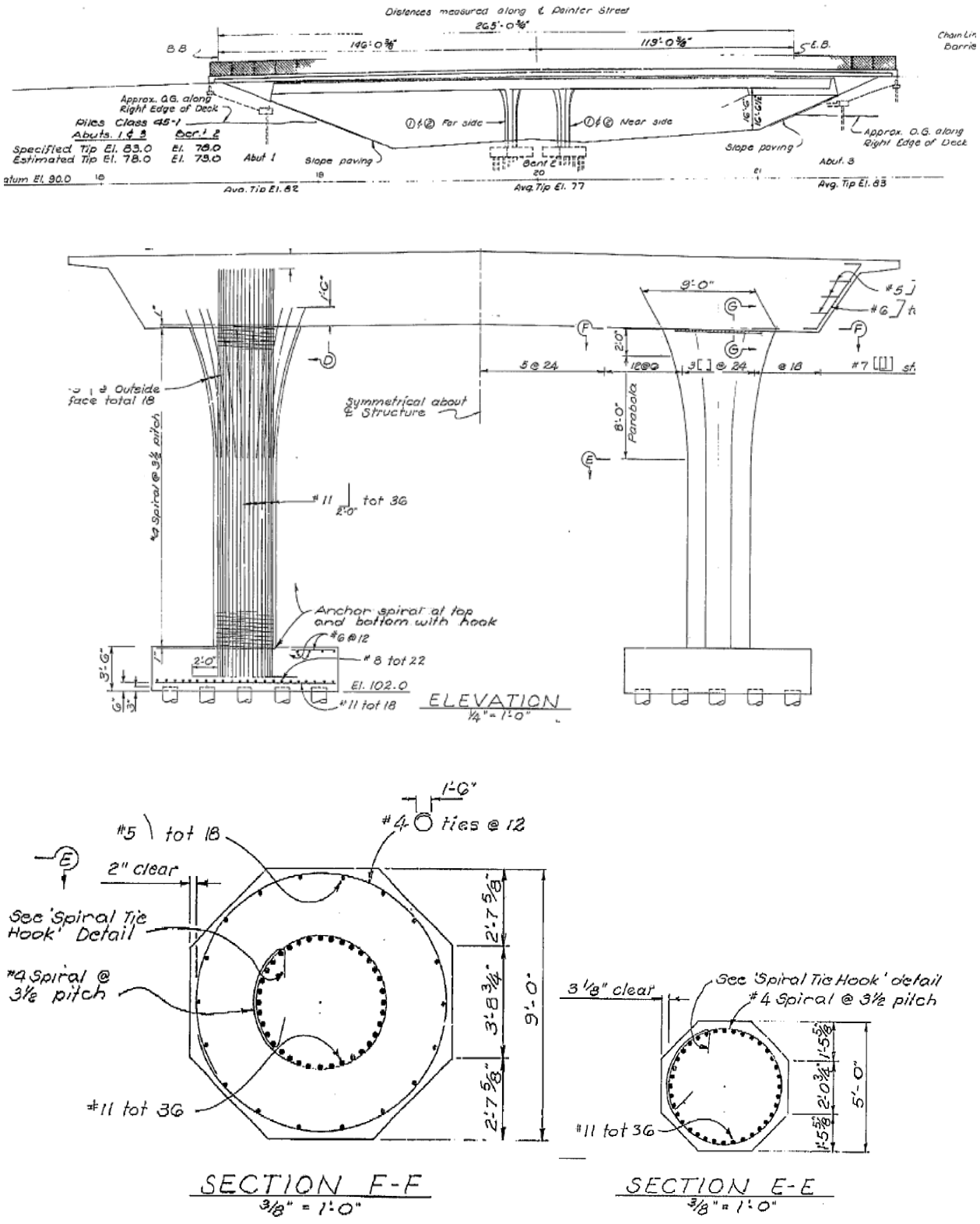

Figure 10. Elevation, deck and column dimensions, and column-section details of the skew-bridge.

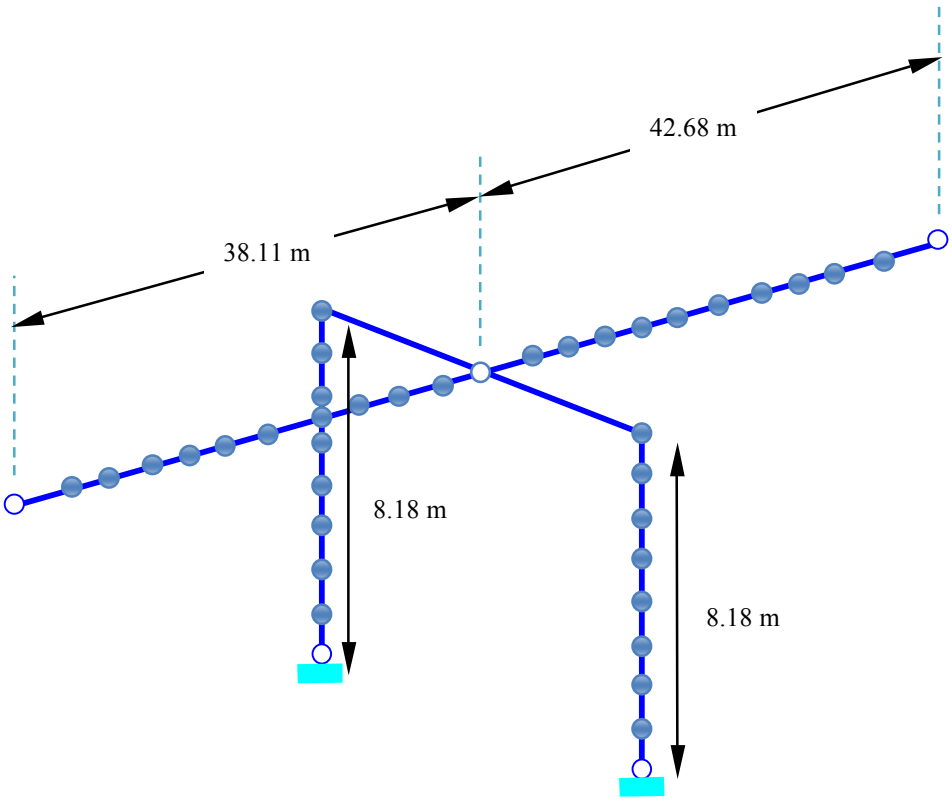

Figure 11. Idealized computer model of the skew-bridge.

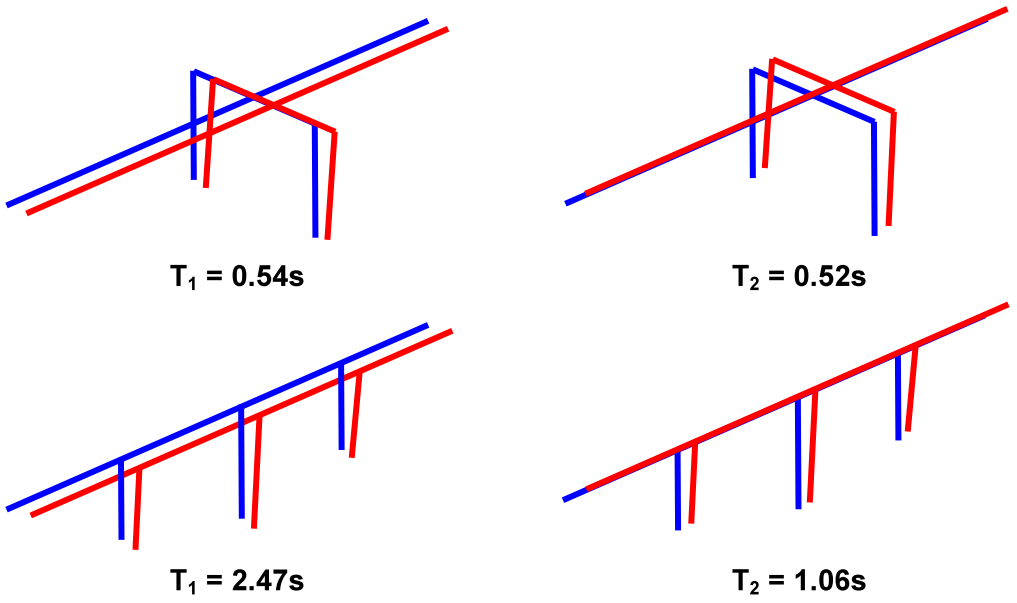

Figure 12. First two modes of vibration and their periods for the single-bent overpass [top-row] and the multi span bridge [bottom-row].

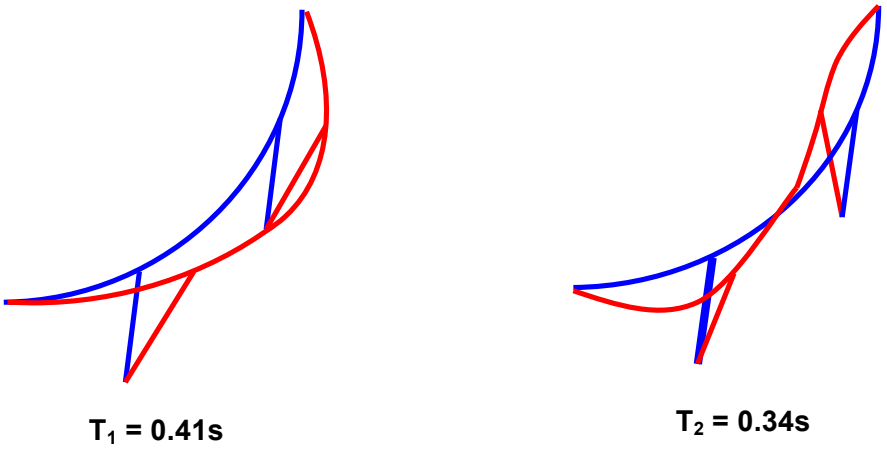

Figure 13. First two modes of vibration and their periods for the curved-bridge.

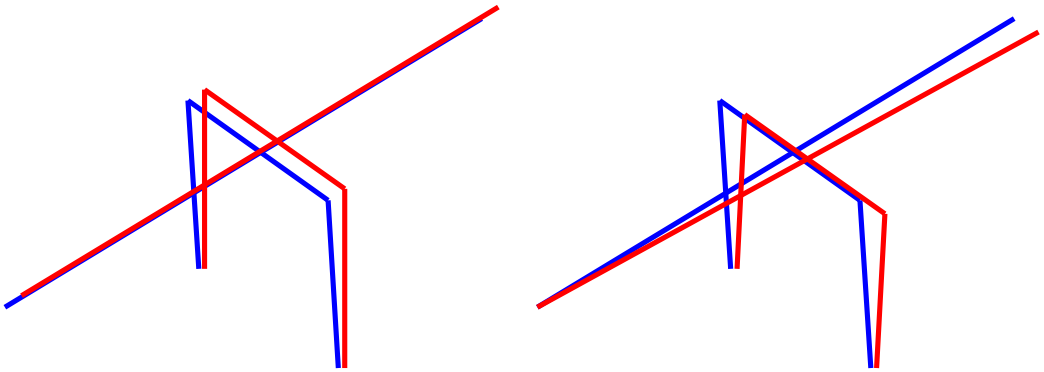

Figure 14. First two modes of vibration and their periods for the skew-bridge.

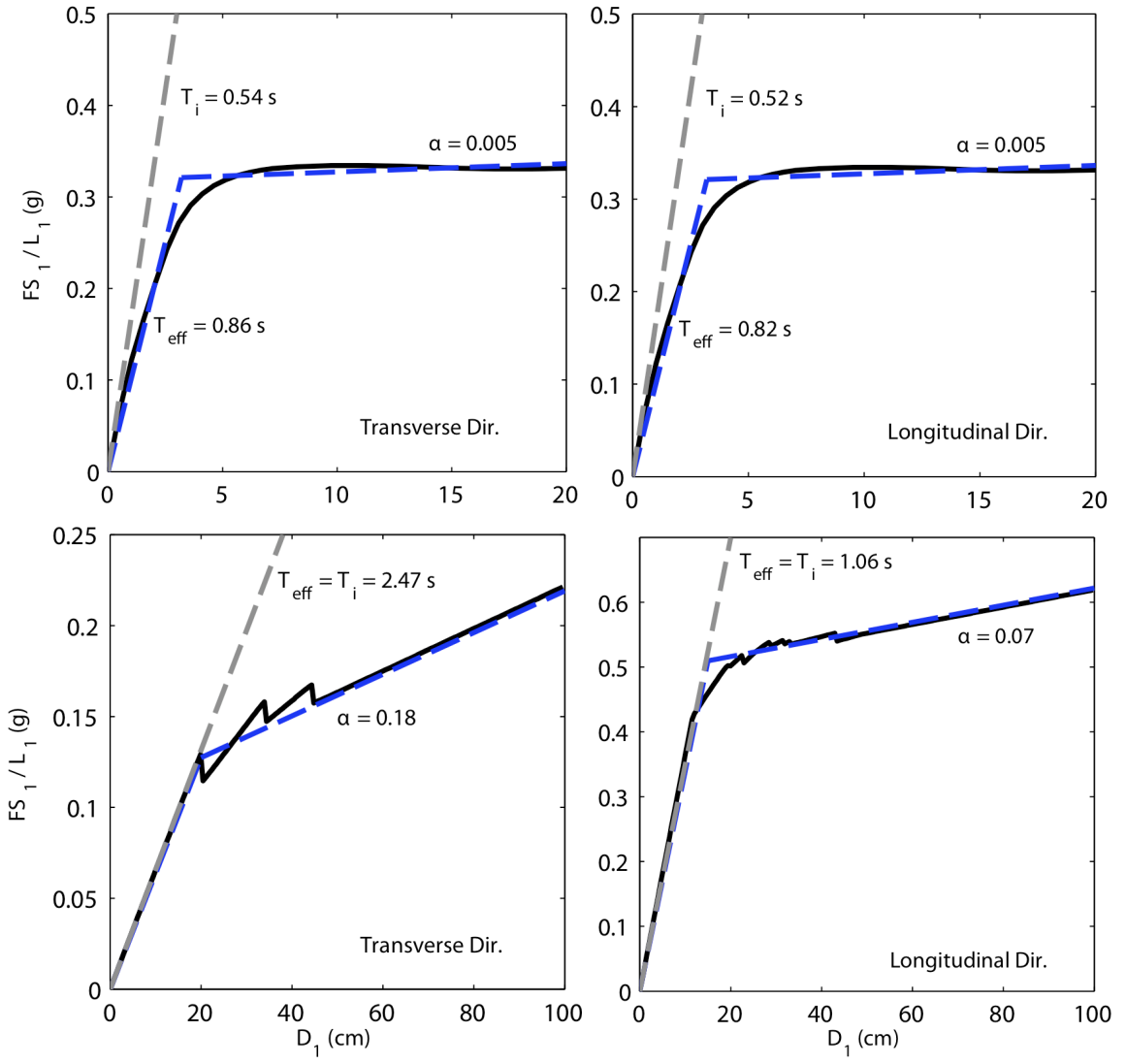

Figure 15. First-"mode" single-degree-of-freedom (SDF) pushover curve (solid line) and its idealized bilinear model (dashed line) in transverse and longitudinal directions for the single-bent overpass [top-panels] and multi span bridge [bottom-panels].

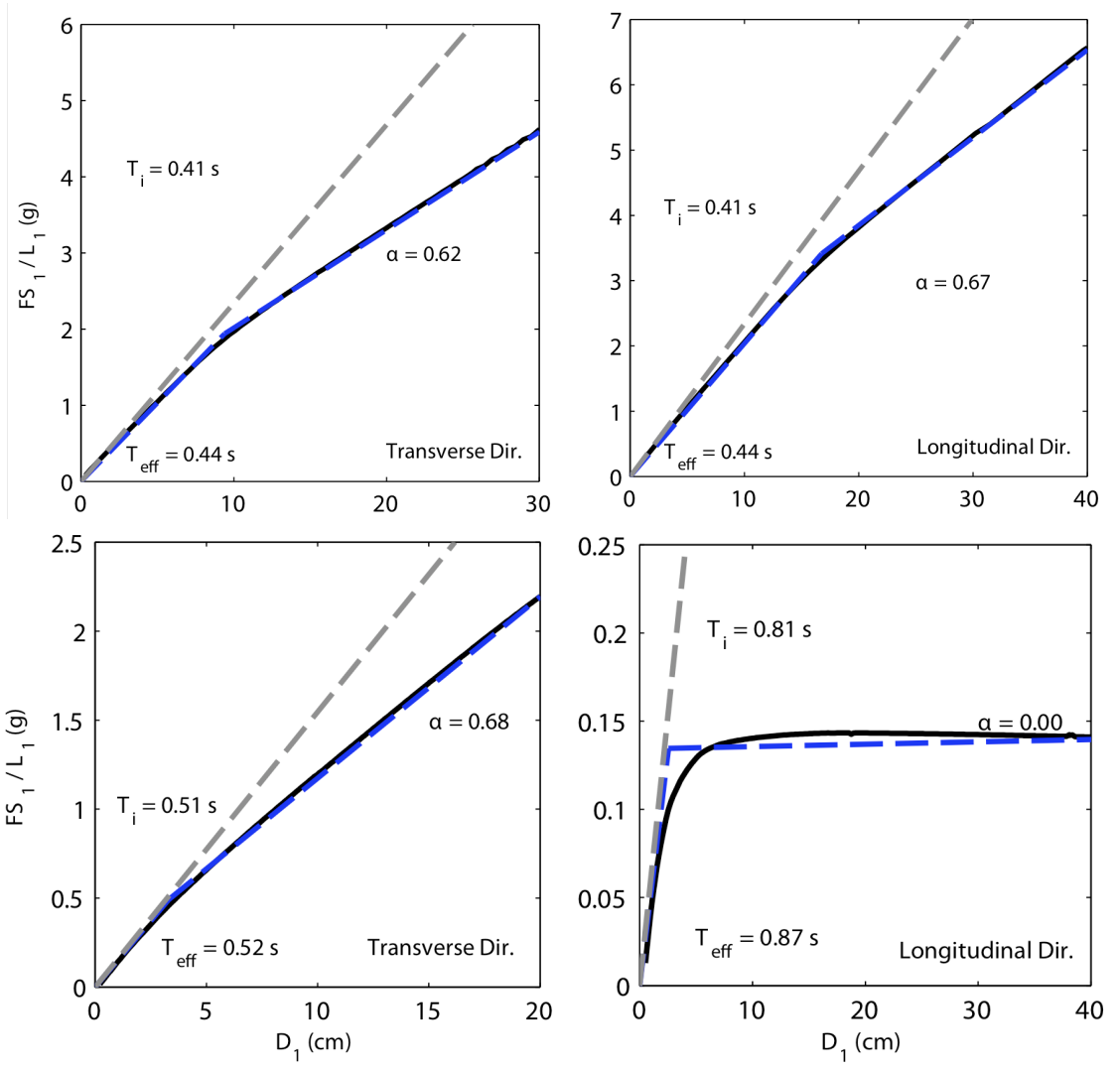

Figure 16. First-"mode" single-degree-of-freedom (SDF) pushover curve (solid line) and its idealized bilinear model (dashed line) in transverse and longitudinal directions for the curved-bridge [top-panels] and skew-bridge [bottom-panels].

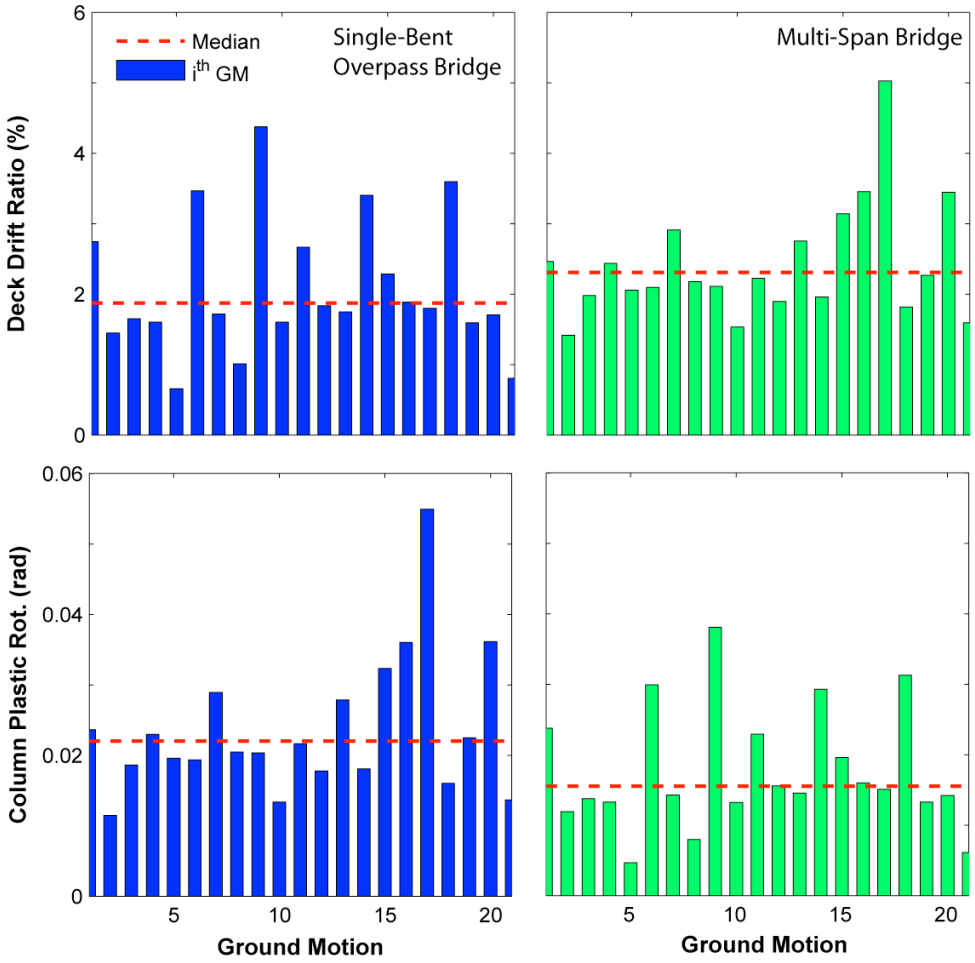

Figure 17. Median values of benchmark engineering demand parameters (EDPs) in transverse direction determined by nonlinear response history analyses (RHA) of the single-bent overpass [left-panels] and multi span bridge [right-panels], due to 21 ground-motion records. Results for individual ground-motion records also are included.

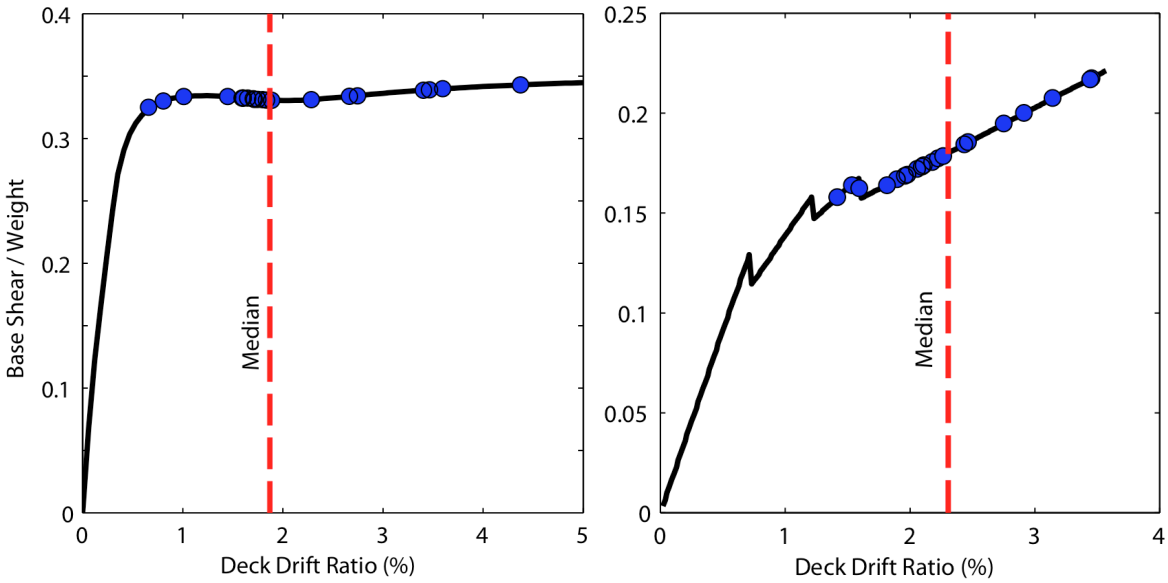

Figure 18. Deck-drift ratios in transverse direction determined by nonlinear response history analyses (RHA) of the single-bent overpass [left] and multi span bridge [right] for 21 ground-motion records identified on first-"mode" pushover curve.

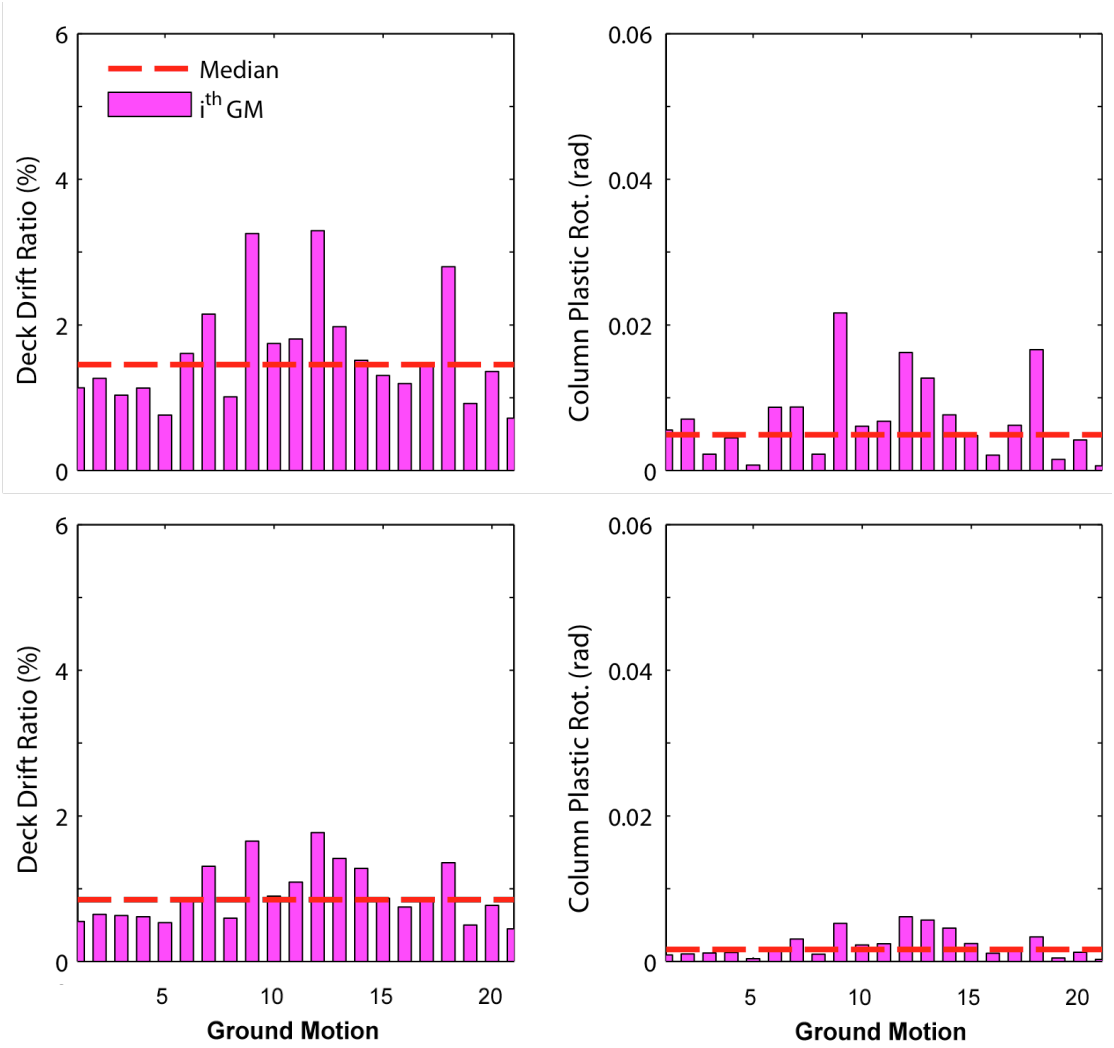

Figure 19. Median values of benchmark engineering demand parameters (EDPs) in transverse direction [top panels] and EDPs in longitudinal direction [bottom panels] determined by nonlinear response history analyses (RHA) of the curved-bridge due to 21 ground-motion records. Results for individual ground-motion records also are included.

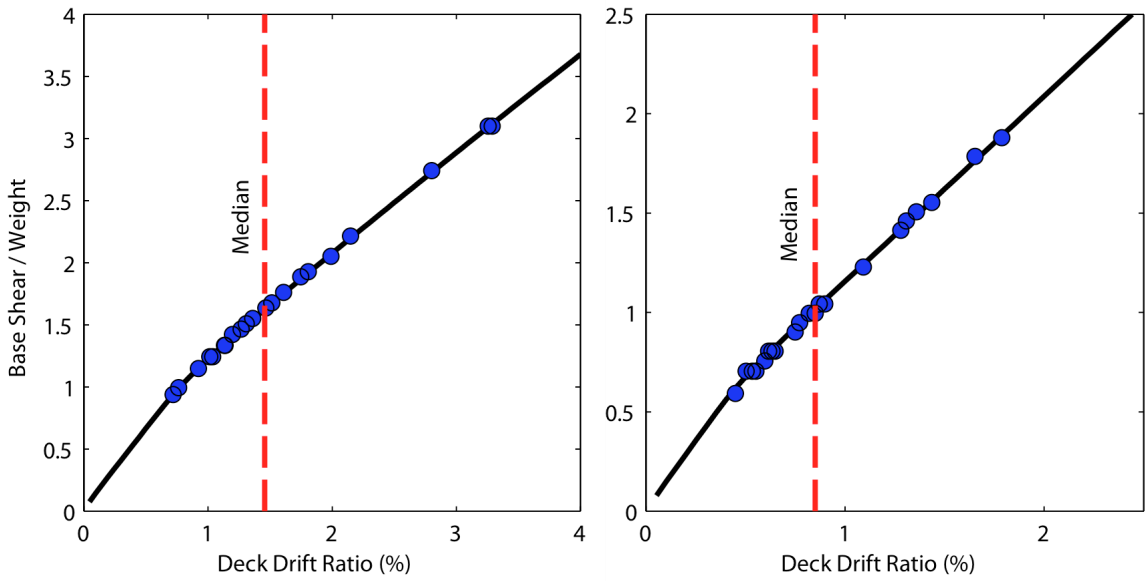

Figure 20. Deck-drift ratios in transverse direction [left] and in longitudinal direction [right] determined by nonlinear response history analyses (RHA) of the curved-bridge for 21 ground-motion records identified on first-"mode" pushover curve in the respective directions.

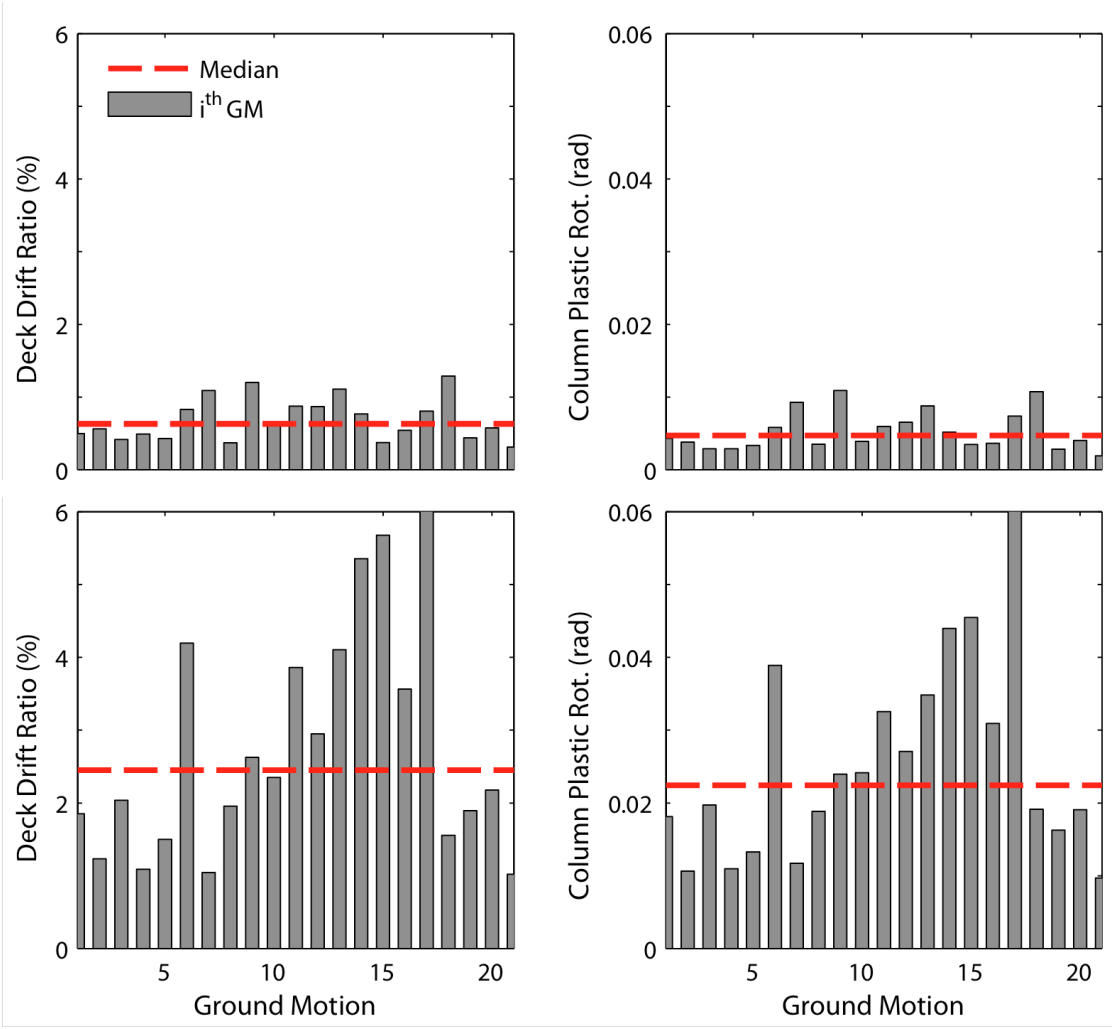

Figure 21. Median values of benchmark engineering demand parameters (EDPs) in transverse direction [top panels] and EDPs in longitudinal direction [bottom panels] determined by nonlinear response history analyses (RHA) of the skew-bridge due to 21 ground-motion records. Results for individual ground-motion records also are included.

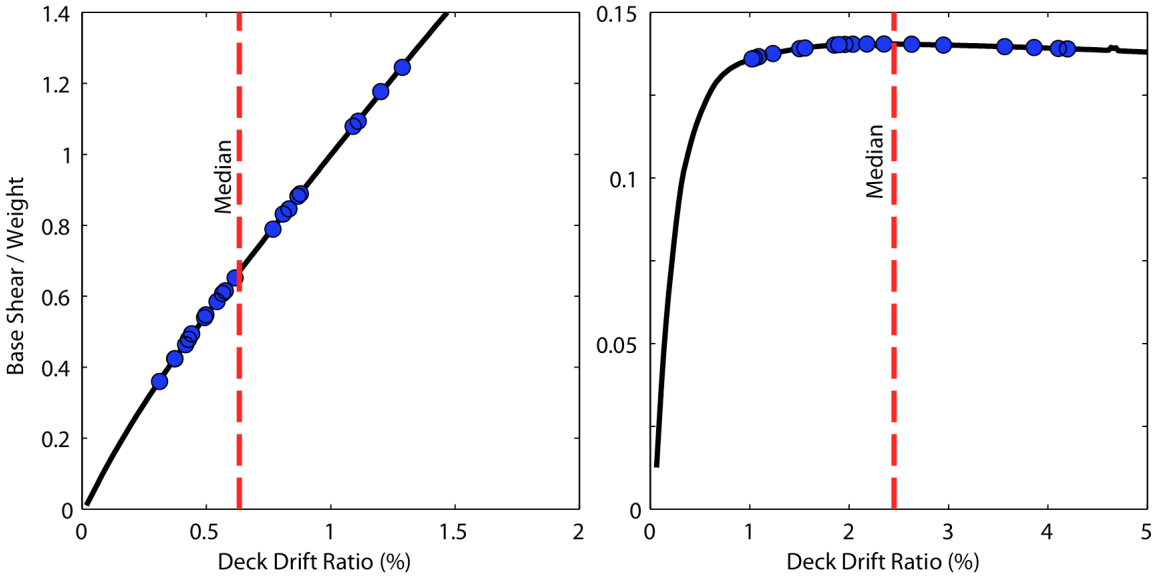

Figure 22. Deck-drift ratios in transverse direction [left] and in longitudinal direction [right] determined by nonlinear response history analyses (RHA) of the skew-bridge for 21 ground-motion records identified on first-"mode" pushover curve in the respective directions.

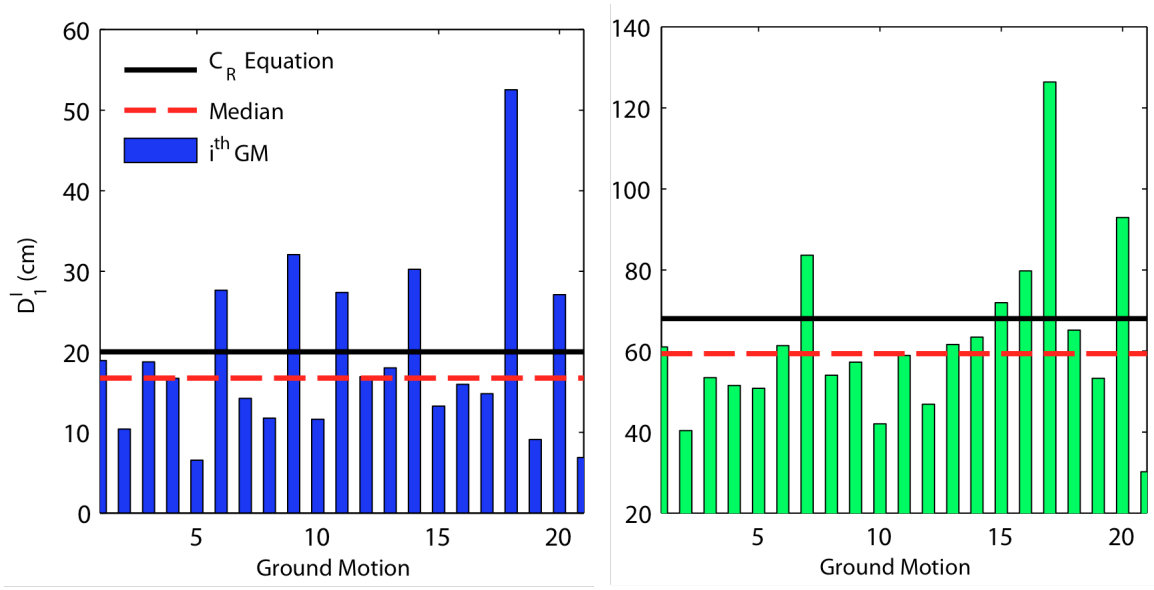

Figure 23. Peak deformation D_1^I values of the first-"mode" inelastic SDF system for 21 ground-motion records for the single-bent overpass [left] and multi span bridge [right]; "exact" target value of deformation $\bar{D}_1^I$ is identified by horizontal dashed line; horizontal continuous line indicates target value of deformation $\bar{D}_1^I$ established by the C_R equation.

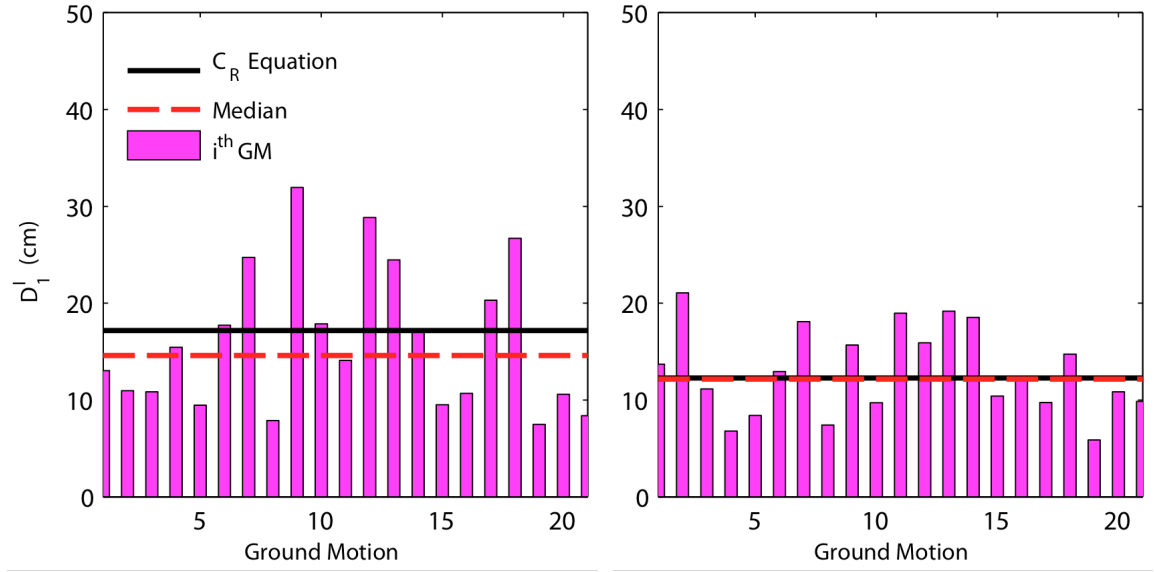

Figure 24. Peak deformation D_1^I values of the first-"mode" inelastic SDF system in the transverse direction [left] and in the longitudinal direction [right] for 21 ground-motion records for the curved-bridge; "exact" target value of deformation $\bar{D}_1^I$ is identified by horizontal dashed line; horizontal continuous line indicates target value of deformation $\bar{D}_1^I$ established by the C_R equation.

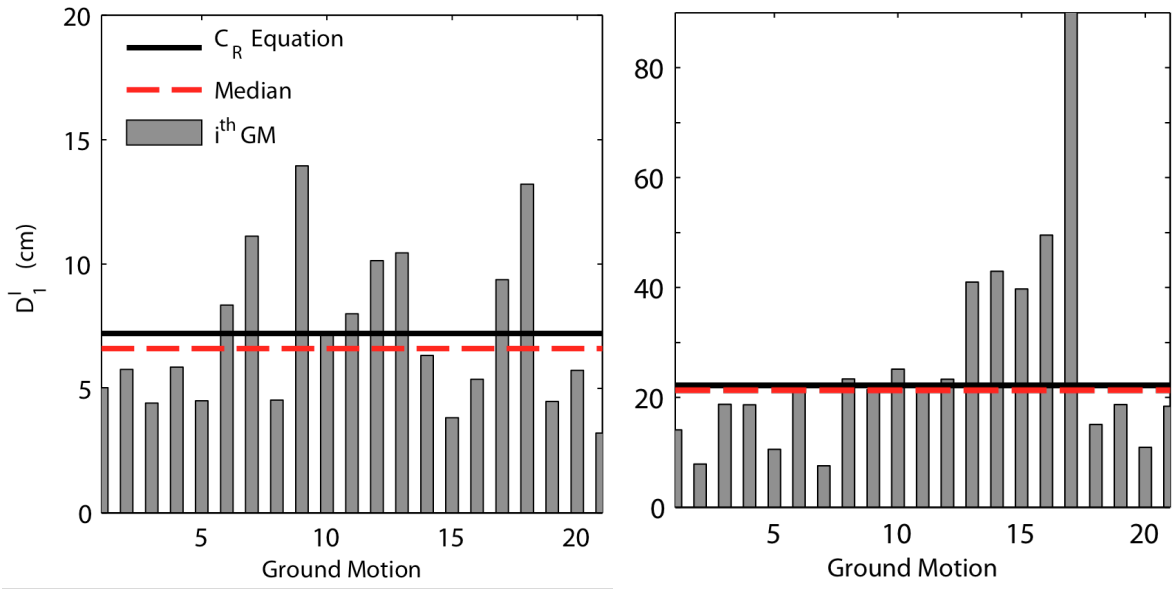

Figure 25. Peak deformation D_1^I values of the first-"mode" inelastic SDF system in the transverse direction [left] and in the longitudinal direction [right] for 21 ground-motion records for the skew-bridge; "exact" target value of deformation $\bar{D}_1^I$ is identified by horizontal dashed line; horizontal continuous line indicates target value of deformation $\bar{D}_1^I$ established by the C_R equation.

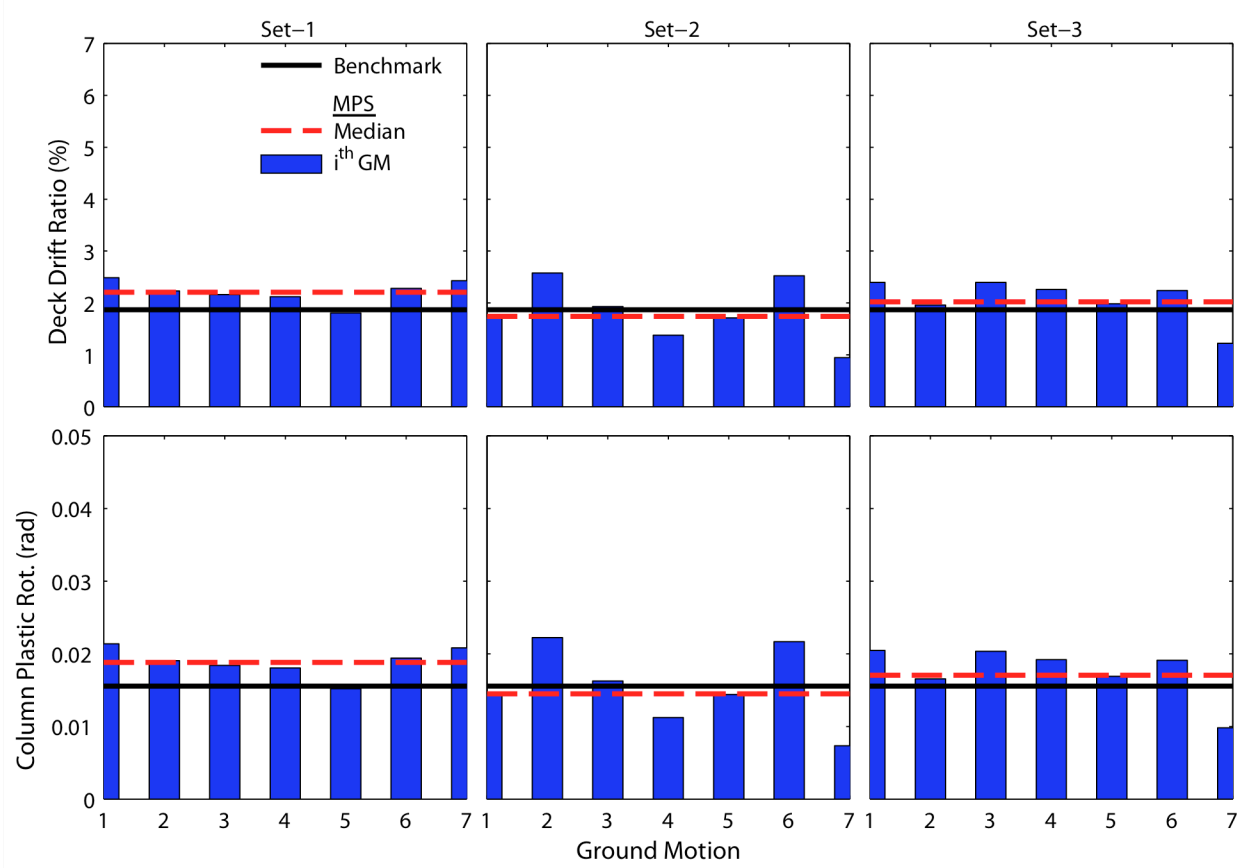

Figure 26. Comparison of median engineering demand parameters (EDPs) based on the modal pushover-based scaling (MPS) procedure with benchmark EDPs for the single-bent overpass; individual results for each of the seven scaled ground-motion records also are presented.

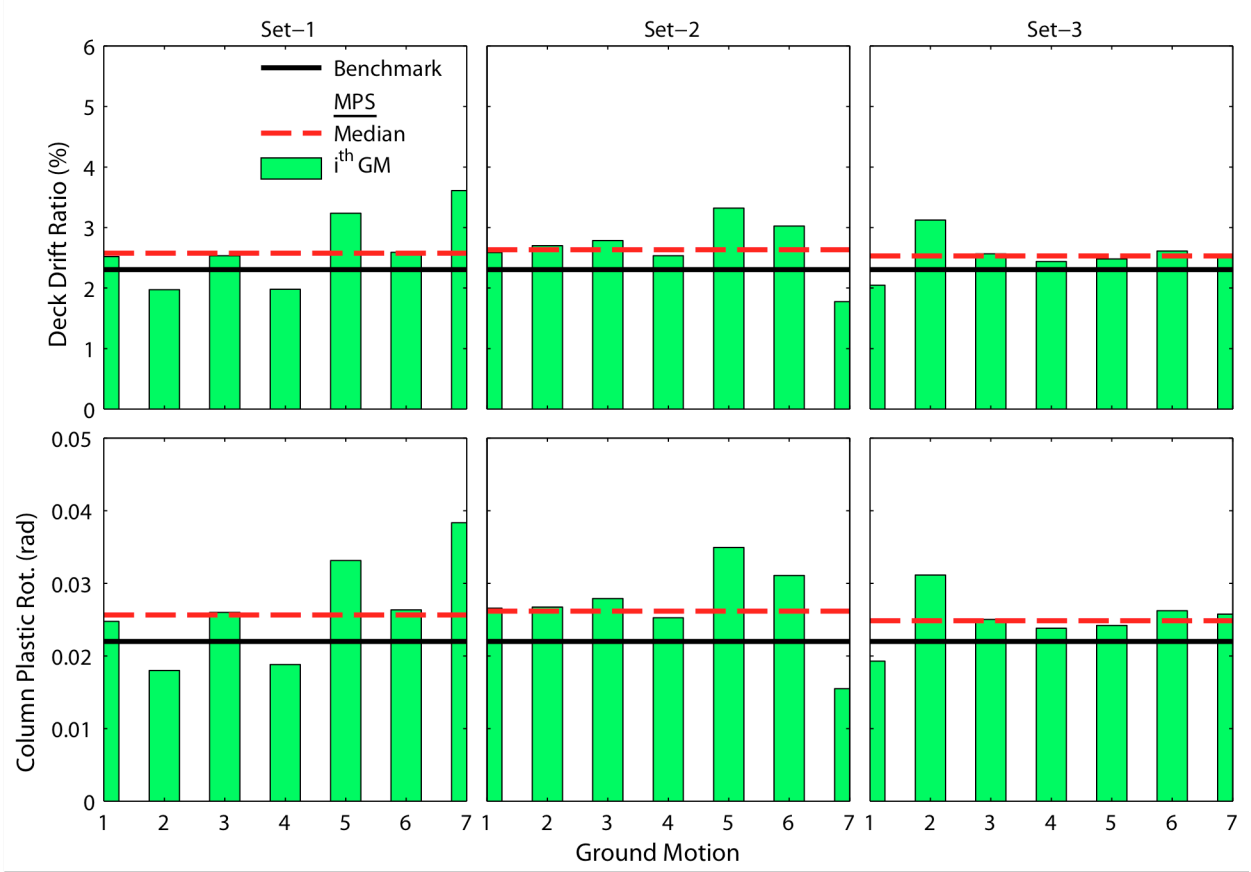

Figure 27. Comparison of median engineering demand parameters (EDPs) based on the modal pushover-based scaling (MPS) procedure with benchmark EDPs for the multi span bridge; individual results for each of the seven scaled ground-motion records also are presented.

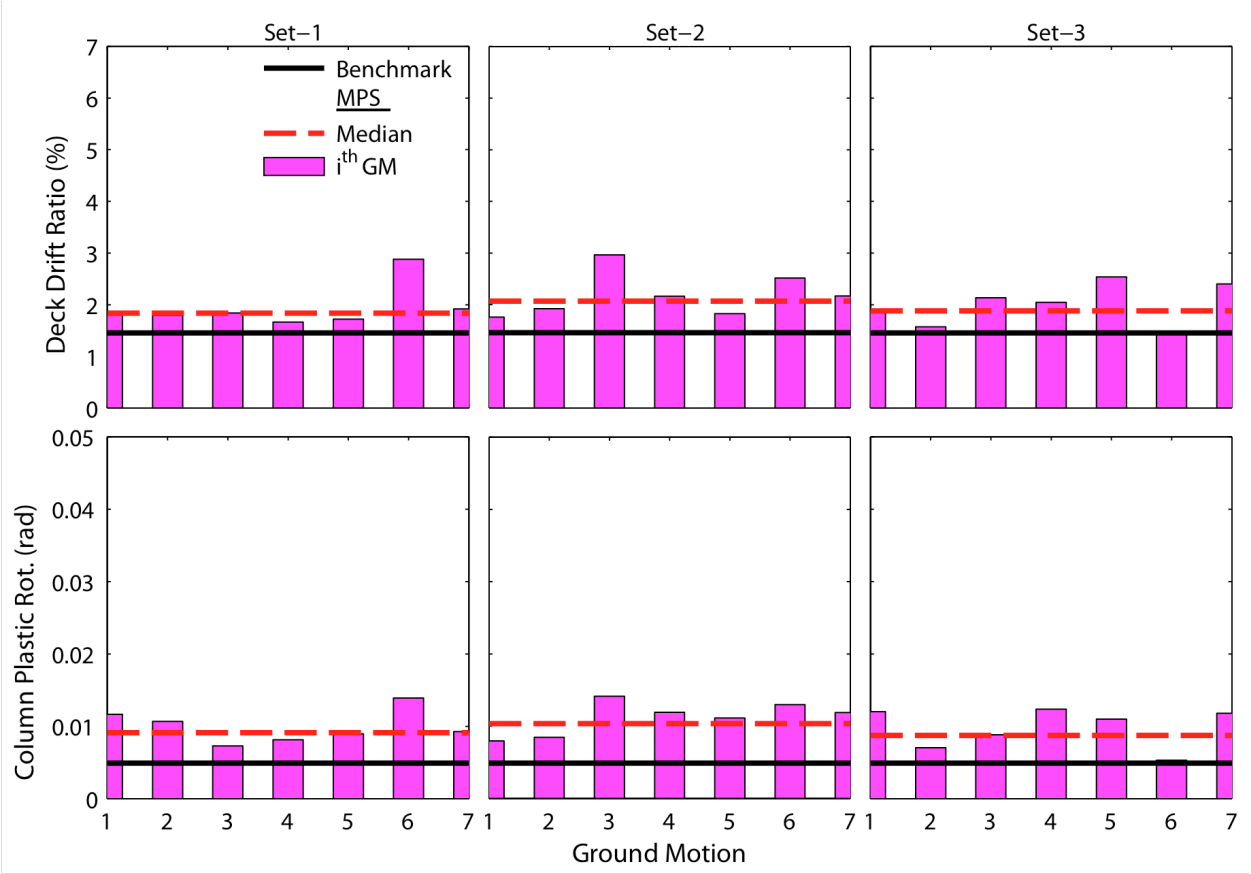

Figure 28. Comparison of median engineering demand parameters (EDPs) based on the modal pushover-based scaling (MPS) procedure with benchmark EDPs for the curved-bridge; individual results for each of the seven scaled ground-motion records also are presented.

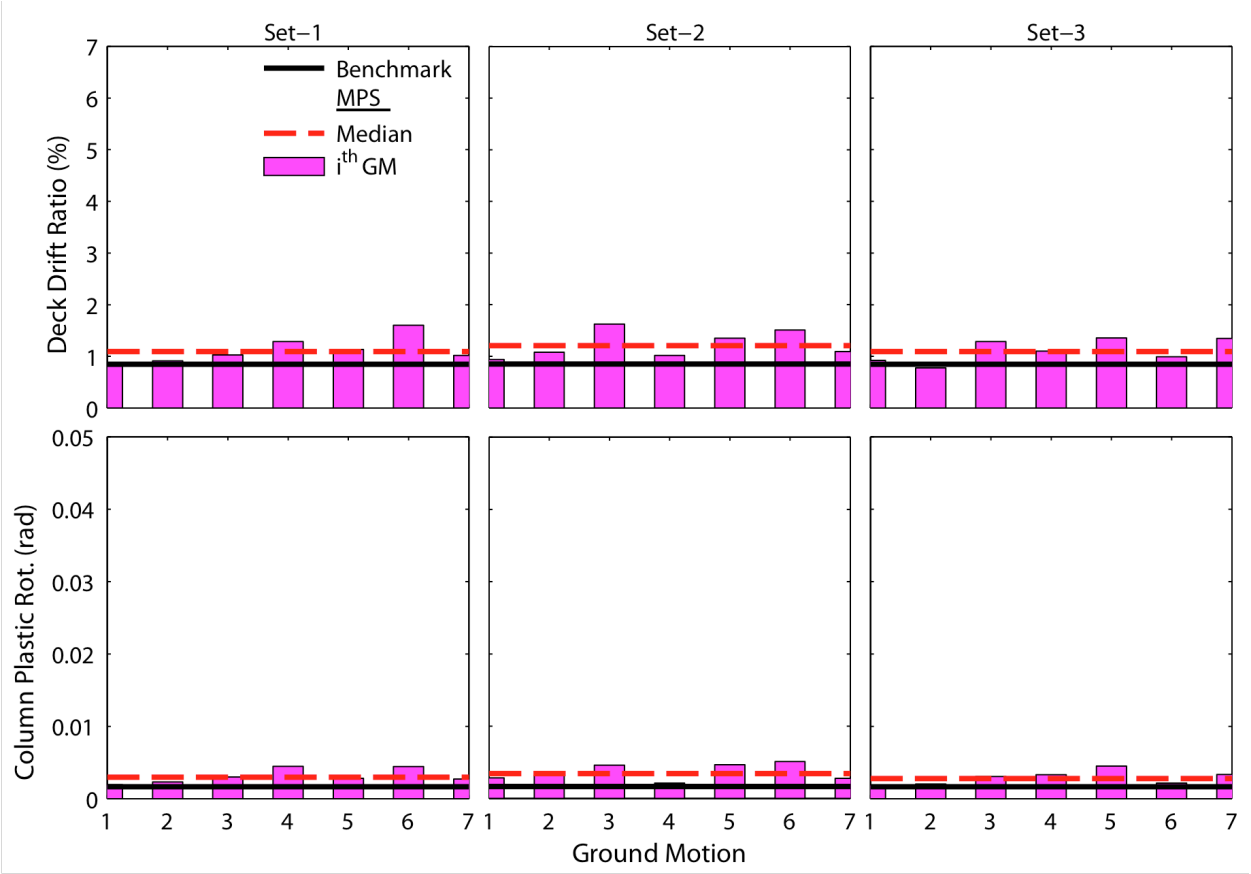

Figure 29. Comparison of median engineering demand parameters (EDPs) based on the modal pushover-based scaling (MPS) procedure with benchmark EDPs for the curved-bridge; individual results for each of the seven scaled ground-motion records also are presented.

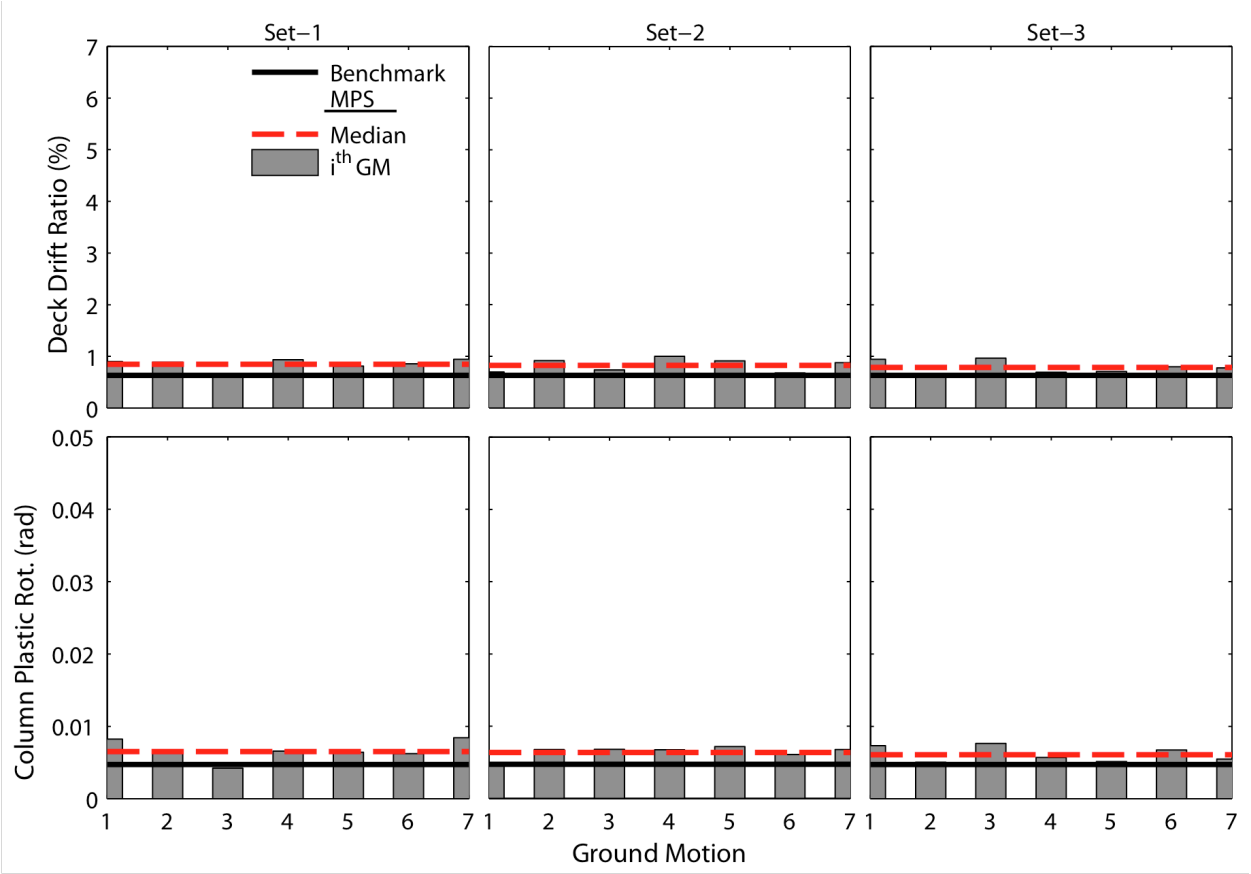

Figure 30. Comparison of median engineering demand parameters (EDPs) based on the modal pushover-based scaling (MPS) procedure with benchmark EDPs for the skew-bridge; individual results for each of the seven scaled ground-motion records also are presented.

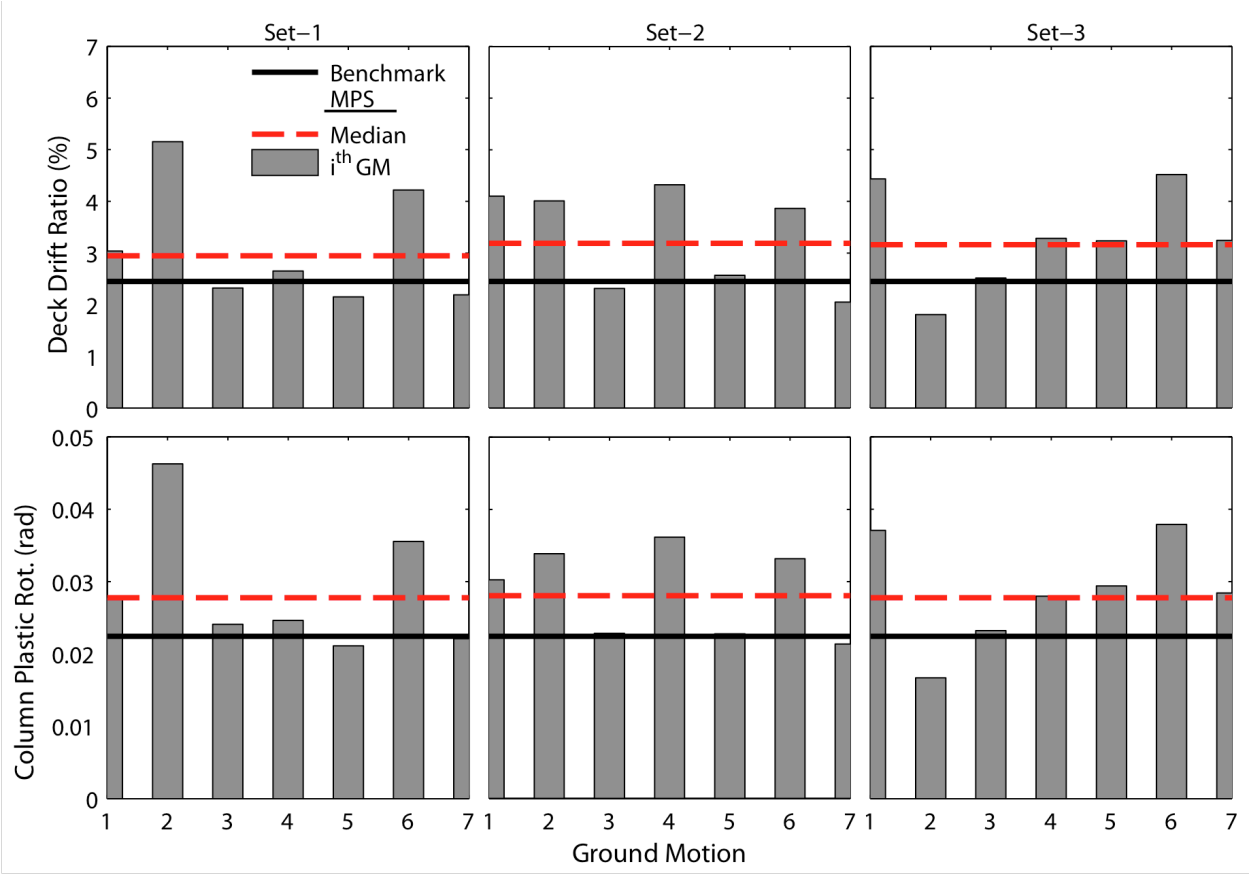

Figure 31. Comparison of median engineering demand parameters (EDPs) based on the modal pushover-based scaling (MPS) procedure with benchmark EDPs for the skew-bridge; individual results for each of the seven scaled ground-motion records also are presented.

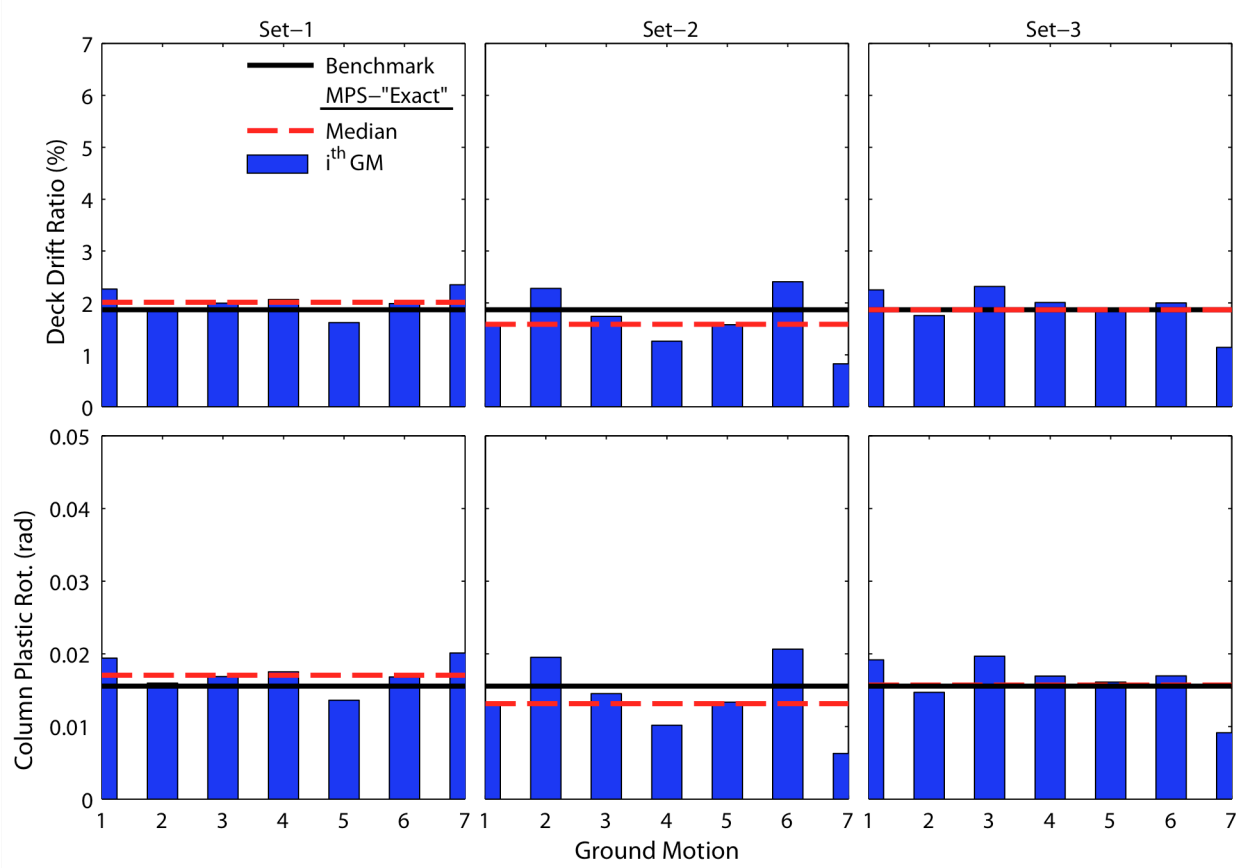

Figure 32. Comparison of median engineering demand parameters (EDPs) based on the modal pushover-based (MPS) "Exact" procedure with benchmark for the single-bent overpass; individual results for each of the seven scaled ground-motion records also are presented.

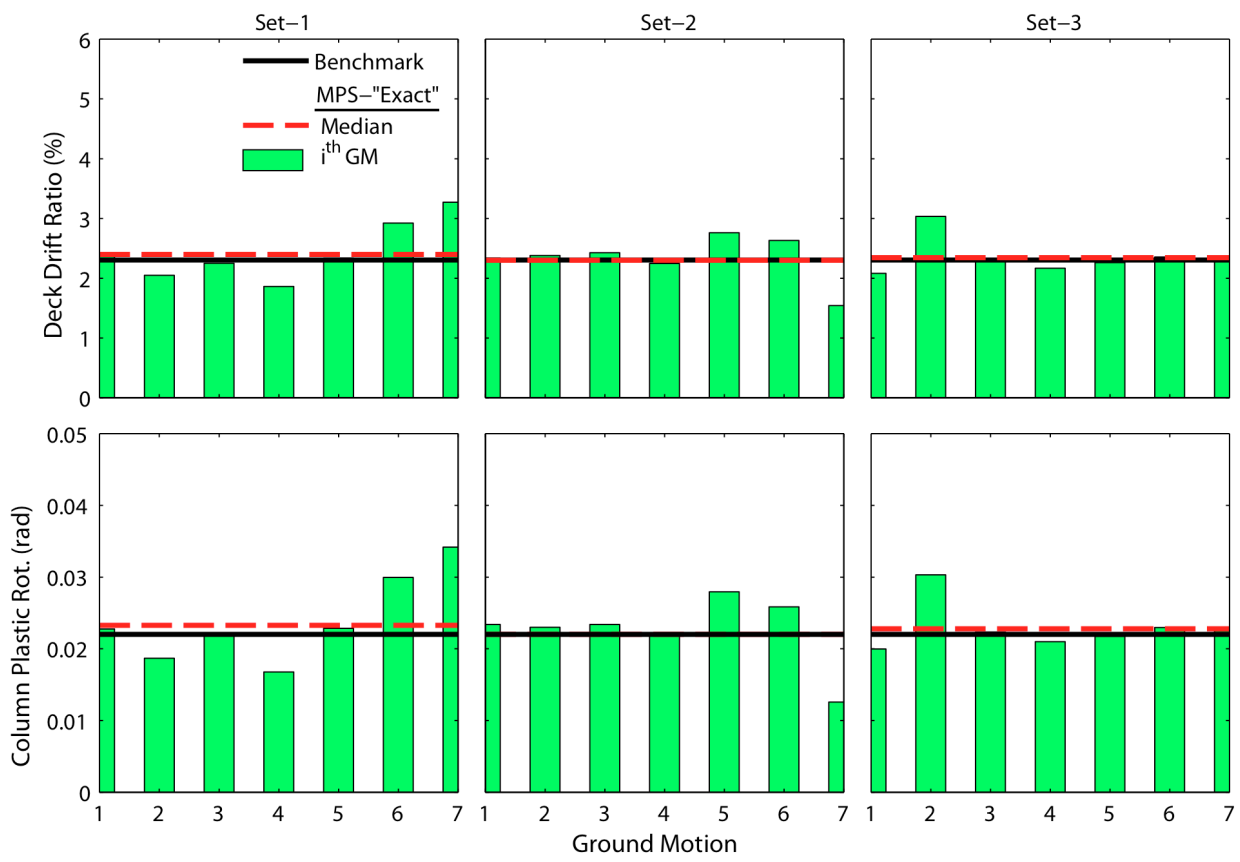

Figure 33. Comparison of median engineering demand parameters (EDPs) based on the modal pushover-based (MPS) "Exact" procedure with benchmark EDPs for the multi span bridge; individual results for each of the seven scaled ground-motion records also are presented.

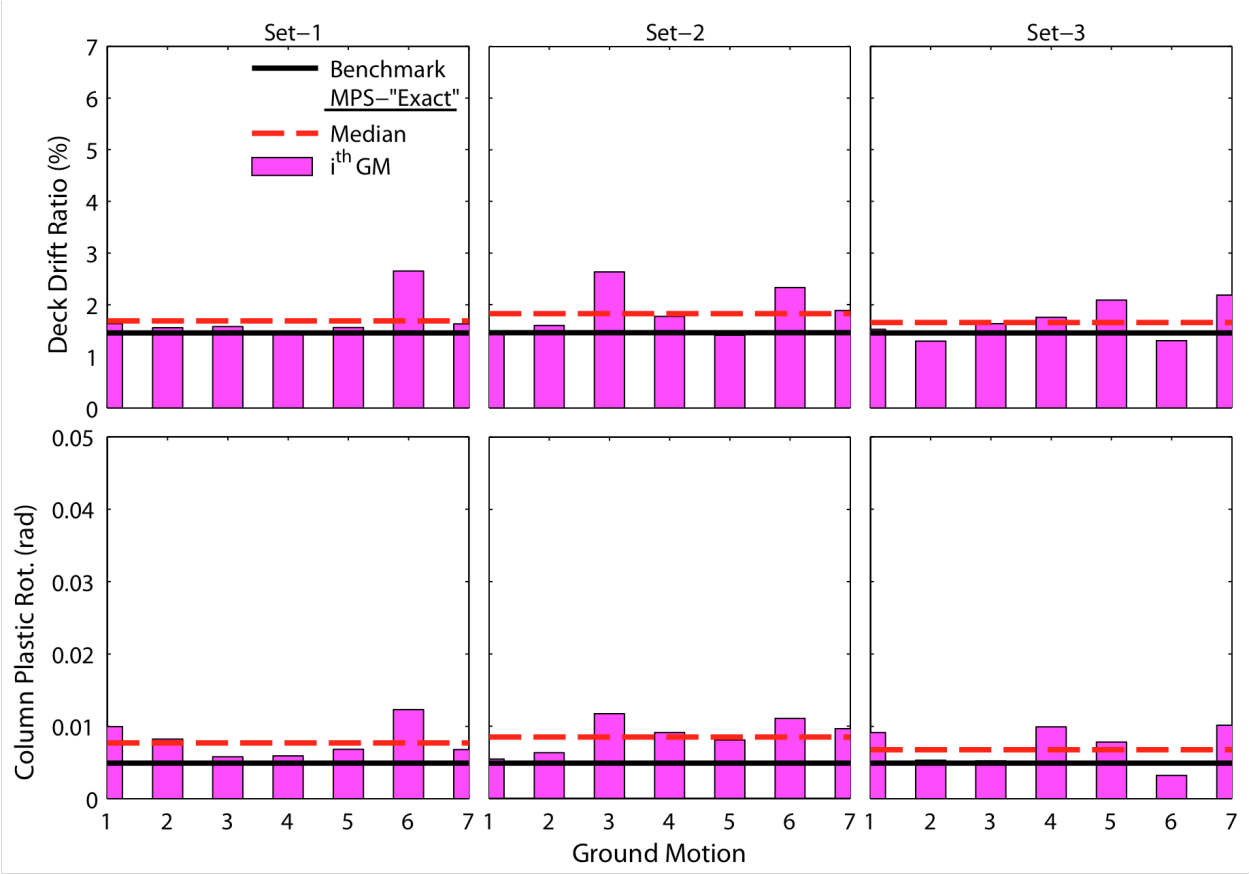

Figure 34. Comparison of median engineering demand parameters (EDPs) based on the modal pushover-based (MPS) "Exact" procedure with benchmark EDPs for the curved-bridge; individual results for each of the seven scaled ground-motion records also are presented.

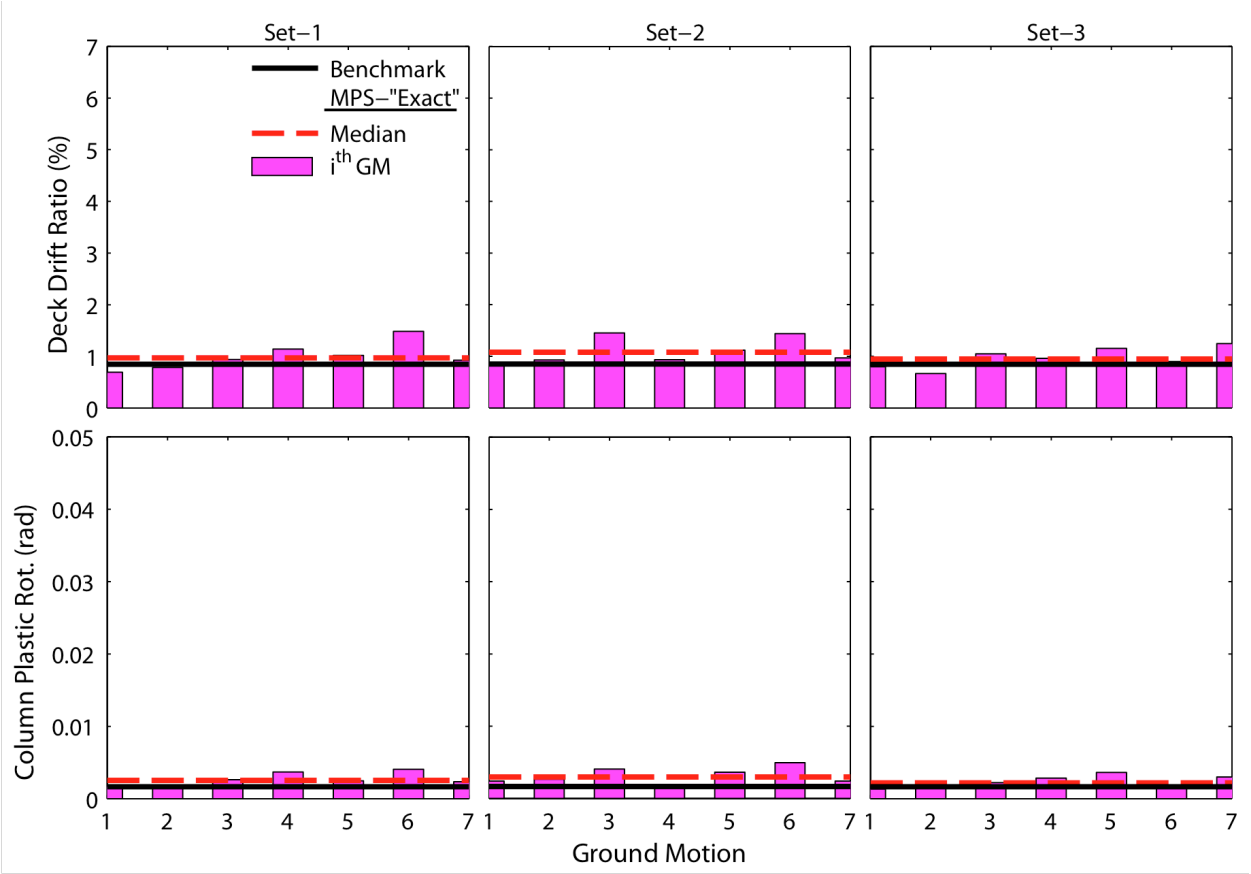

Figure 35. Comparison of median engineering demand parameters (EDPs) based on the modal pushover-based (MPS) "Exact" procedure with benchmark EDPs for the curved-bridge; individual results for each of the seven scaled ground-motion records also are presented.

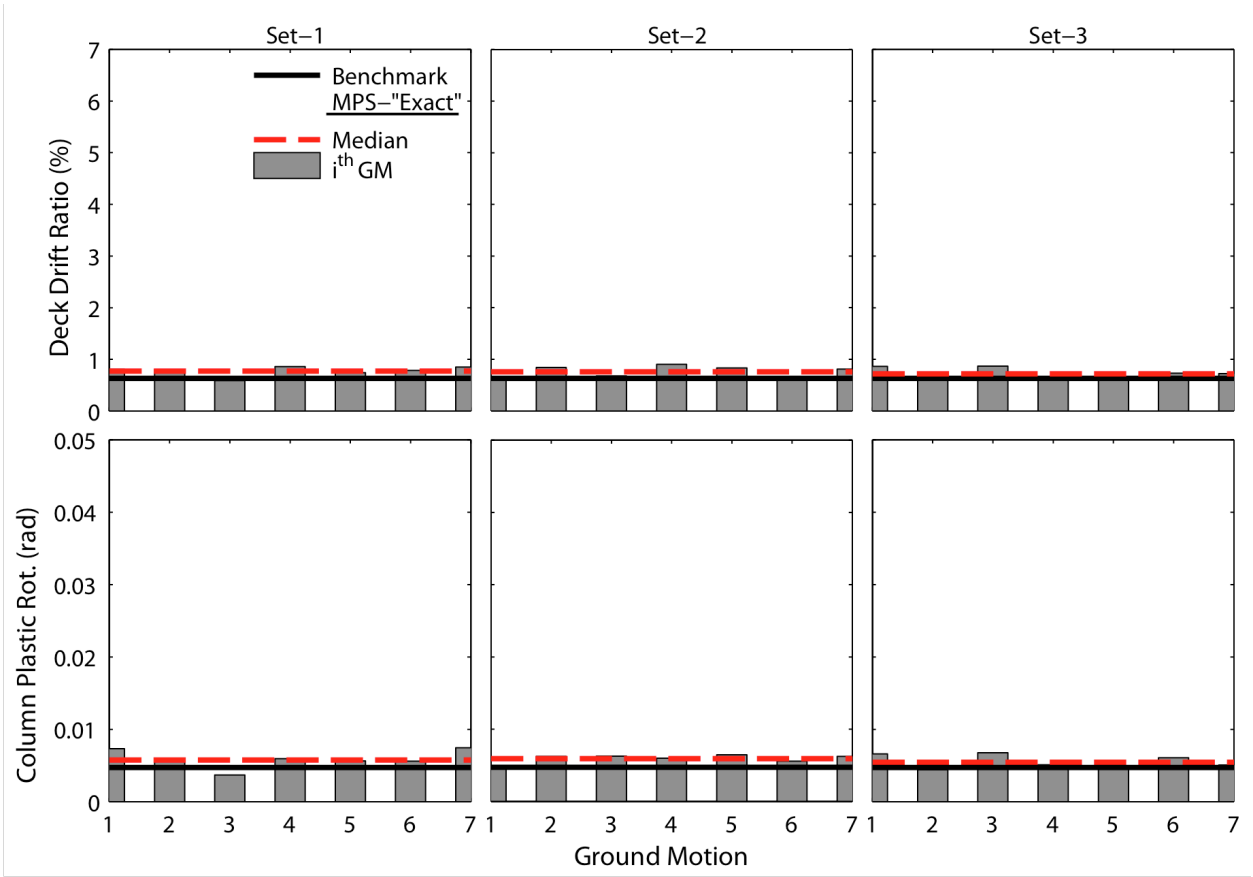

Figure 36. Comparison of median engineering demand parameters (EDPs) based on the modal pushover-based (MPS) "Exact" procedure with benchmark EDPs for the skew-bridge; individual results for each of the seven scaled ground-motion records also are presented.

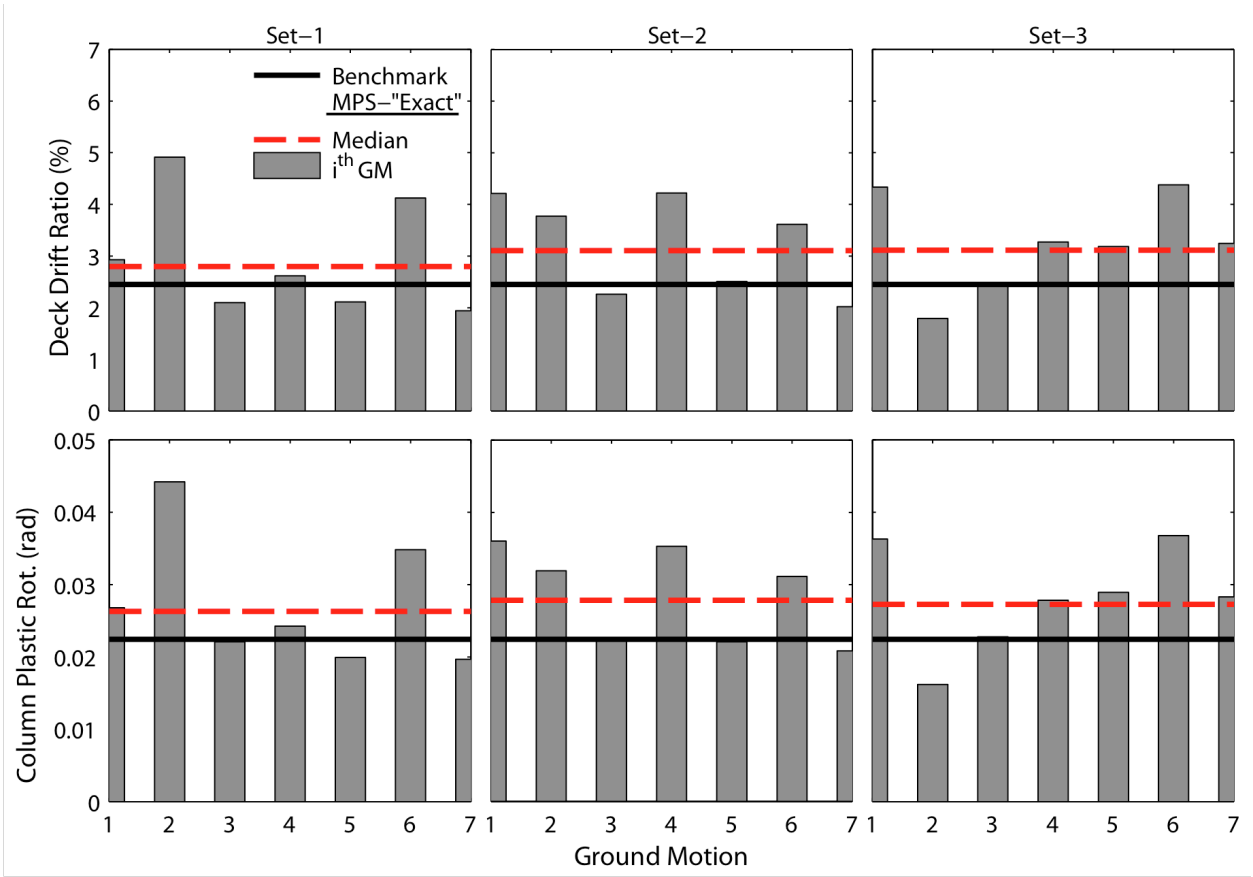

Figure 37. Comparison of median engineering demand parameters (EDPs) based on the modal pushover-based (MPS) "Exact" procedure with benchmark EDPs for the skew-bridge; individual results for each of the seven scaled ground-motion records also are presented.